Universidade de Aveiro
2018

Departamento de Ciências Médicas

Beatriz Soares Carneiro da Silva

A interação entre o citomegalovírus humano e os peroxissomas: metabolismo e associação membranar com o retículo endoplasmático

The interplay between cytomegalovirus and peroxisomes: metabolism and membrane association with the endoplasmic reticulum

Universidade de Aveiro
2018

Departamento de Ciências Médicas

Beatriz Soares Carneiro da Silva

A interação entre o citomegalovírus humano e os peroxissomas: metabolismo e associação membranar com o retículo endoplasmático

The interplay between human cytomegalovirus and peroxisomes: metabolism and membrane association with the endoplasmic reticulum

Tese apresentada à Universidade de Aveiro para cumprimento dos requisitos necessários à obtenção do grau de Mestre em Biomedicina Molecular, realizada sob a orientação científica da Dr. Daniela Maria Oliveira Gandra Ribeiro, Investigadora do Departamento de Ciências Médicas da Universidade de Aveiro e Investigadora Principal do grupo "Organelle Dynamics in Infection and Disease" do Instituto de Biomedicina (iBiMED), Universidade de Aveiro.

Thesis submitted at University of Aveiro to fulfil the requirements to obtain the Master's Degree in Molecular Biomedicine, held under the scientific guidance of Dr. Daniela Maria Oliveira Gandra Ribeiro, Researcher at Medical Sciences Department of University of Aveiro and Principal Investigator at Organelle Dynamics in Infection and Disease group at Institute for Biomedicine (iBiMED), University of Aveiro.

PTDC/BIACEL/31378/2017 (POCI-01-0145-FEDER-031378) através do Programa Operacional Competitividade e Internacionalização (COMPETE2020). Cofinanciado pelo Fundo Comunitário Europeu FEDER e Fundação para a Ciência e Tecnologia (FCT).

Dedico esta tese à minha família.

o júri

presidente

Doutor Bruno Miguel Rodrigues das Neves
Professor Auxiliar em Regime Laboral do Departamento de Ciências Médicas da Universidade de Aveiro

Doutora Daniela Maria Oliveira Gandra Ribeiro
Investigadora do Departamento de Ciências Médicas da Universidade de Aveiro e Investigadora Principal do grupo “Organelle Dynamics in Infection and Disease” do Instituto de Biomedicina da Universidade de Aveiro

Doutora Ana Sofia da Cunha Guimarães
Investigadora de Pós-doutoramento do Instituto de Biologia Molecular e Celular do Instituto de Investigação e Inovação em Saúde da Universidade do Porto

agradecimentos

After a year and a half of working in this thesis I must thank to every person that I met and contributed to each step that I took and that supported me in all situations.

To Dr. Daniela Ribeiro for all the knowledge that shared with me, for letting me be part of such interesting work that it is developed in the lab and all the enthusiasm that infected me every time. For showing me how great this job can be even in bad days and for always pushing me to be better.

To my work group, that allowed that this work could be possible. To Isabel, for sharing with me her detailed knowledge and for all the support, jokes and outbursts. To Rita, for helping me in everything, in work and in general life. To Mariana, for all the help, for all the support, for all the jokes, in short, for all the love. To Catarina, for the companion, for listen to my worries, for all the friendship and for always being there professional and personally. To Rui, for being a great mate on this adventure.

To Carolina, for all the help, for being my SOS person and specially for the friendship.

To Dr. Markus Islinger and his incredible group that received me with their open arms, shared with me all their knowledge and allowing that in just four months I had a great experience.

To Dr. Alexandra Nunes and Sandra Magalhães for all the patience that had with me and for all the help with FTIR spectroscopy.

To my class mates that contributed for two great years. A special thanks to you, Flávia for the help to go through all the good and bad things and for being a great friend. And to you Teixeira, for being an amazing friend, for the support, for the videochats, for the dinners, for the companion and for always being there.

To my long date friends for all the cafes, for pulling up with all my virus talk, for all the fun, for being my “distraction moment” and for being my best friends after so many years.

And finally, but not least, a very special thanks to my mom, dad, siblings and family. Without you nothing of this was possible. Thank you for putting up with all my bad days, for the interest on my work, for all the support and for being simply amazing.

palavras-chave

peroxissomas, resposta antiviral celular, imunidade inata celular, RIG-I, vMIA, citomegalovírus humano, comunicação inter-organelos, ACBD5, retículo endoplasmático

resumo

Os peroxissomas são organelos que desempenham funções metabólicas essenciais para as células, nomeadamente a β-oxidação de ácidos gordos de cadeia longa, síntese de fosfolípidos, manutenção dos níveis celulares de espécies reativas de oxigénio.

Os peroxissomas também foram descritos como plataformas de sinalização na via antiviral dos recetores RIG-I-like (RLR). Após infeção, o ARN viral é libertado para o citoplasma onde é reconhecido pelos recetores RLR, que na superfície das mitocôndrias e dos peroxissomas induzem a ativação da MAVS. A ativação da MAVS leva a uma cascata de sinalização que culmina com a produção de interferões e genes estimulados pelos interferões.

Os peroxissomas estabelecem interações com diversos organelos para manter a homeostase celular. Uma destas interações inter-organelos é a relação com o retículo endoplasmático. Os peroxissomas dependem do retículo endoplasmático para a sua biogénese, e recentemente foi descrito que a ACBD5, uma proteína peroxissomal conhecida por mediar o importe de lípidos para os peroxissomas, interage com a VAPB, uma proteína do retículo endoplasmático.

Neste trabalho, nós estudamos o efeito da ativação da defesa antiviral celular sobre as funções metabólicas peroxissomais. Além disso, nós desvendamos a influência da interação inter-organelos entre os peroxissomas e o retículo endoplasmático. Os nossos resultados sugerem que as funções metabólicas peroxissomais não são alteradas pela ativação da sinalização antiviral dependente dos peroxissomas. Todavia, nós observamos que a ausência da ACBD5, que impede a interação entre os peroxissomas e o retículo endoplasmático e está associada à troca de lípidos entre os dois organelos, inibe a resposta antiviral.

Estudos futuros para confirmar o papel das funções metabólicas peroxissomais após infeções virais, assim como o efeito da ACBD5 na resposta antiviral celular, em particular na sinalização dependente dos peroxissomas, são propostos.

keywords

peroxisomes, cellular antiviral response, cellular innate immunity, RIG-I, vMIA, human cytomegalovirus, inter-organelle communication, ACBD5, endoplasmic reticulum

abstract

Peroxisomes are organelles responsible for key cellular metabolic functions, such as β-oxidation of very long-chain fatty acids, phospholipid synthesis and cellular redox balance. Peroxisomes have also been described as signalling platforms on the RIG-I-like receptors antiviral pathway. Upon infection, viral RNA is released into the cytoplasm where it is recognized by RIG-I-like receptors, which at the surface of mitochondria and peroxisomes induce the activation of MAVS. MAVS activation leads to a signalling cascade that culminates with the production of interferons and interferons-stimulated genes.

Peroxisomes establish interactions with several organelles to maintain cellular homeostasis. Peroxisomes rely on the endoplasmic reticulum for their biogenesis, and recently it was described that ACBD5, a peroxisomal protein known to mediate the import of lipids into peroxisomes, interacts with VAPB, an endoplasmic reticulum protein. In this work, we study the effect of cellular antiviral defence activation over the peroxisomes metabolic functions. Moreover, we unravel the influence of the interaction between peroxisomes and endoplasmic reticulum.

Our results suggest that peroxisomal metabolic functions are not affected by the activation of the peroxisome-dependent antiviral signalling. Yet, we observe that ACBD5 absence, which impairs interaction between peroxisomes and endoplasmic reticulum and is related with the transference of lipids between both organelles, dampens the antiviral response.

Future studies to confirm the role of peroxisomes metabolic function upon infection, as well as the effect of ACBD5 on the cellular antiviral response, particularly to the peroxisomes-mediated signalling, are proposed.

List of abreviations

ABC Transporters	ATP Binding Cassette Transporters
ABCD1	ATP Binding Cassette Subfamily D member 1
ACAA1	Acetyl-Coenzyme A Acyltransferase 1
ACBD	Acyl-Coenzyme A Binding Domain
ACBD4	Acyl-Coenzyme A-binding domain-containing 4
ACBD5	Acyl-Coenzyme A-binding domain-containing 5
ACBP	Acyl-Coenzyme A-binding protein
Acetyl-CoA	Acetyl-Coenzyme A
ACOX	Acyl-Coenzyme A oxidase 1
Acyl-CoA	Acyl-Coenzyme A
AGPS	Alkyl-Glycerone Phosphate Synthase
AIM2	Absent in Melanoma 2
ALD	Adrenoleukodystrophy
ATF2	Activating Transcription Factor 2
ATPase	Adenosine Triphosphate
ATPase	class of enzymes that catalise ATP
Bak	BCL2 homologous antagonist/killer
Bax	BCL2 associated X
BCL-2	B-cell lymphoma 2
CARD	Caspase Activation and Recruitment Domain
cGAMP	cyclic Guanosine Monophosphate-Adenosine Monophospate
cGAS	cyclic Guanosine Monophosphate-Adenosine Monophospate Synthase
c-Jun	c-Coenzyme c-J
CTDs	C-terminal regulatory domains
DAI	DNA-dependent activator of IFN-regulatory factors
DBP	D-bifunctional proteins
DHAP	DiHydroxyAcetone Phosphate
DHAPAT	DiHydroxyAcetone Phosphate AcylTransferase
DLP1	Dynamin Like Protein 1
DNA	DesoxirriboNucleic Acid
dsDNA	double stranded DesoxirriboNucleic Acid

Enoyl-CoA	Enoyl-Coenzyme A
ER	Endoplasmic Reticulum
Fis1	Fission protein 1
glutaryl-CoA	glutaryl-Coenzyme A
GTPase Drp1/DLP1	dynamin-related GTPase Drp1/DLP1
H_2O_2	Hydrogen Peroxide
HCMV	Human CitoMegalovirus Virus
IE86	HCMV immediate-early protein
IFI16	Gamma-Interferon-Inducible Protein IFI-16
IFNs	Interferons
IKK	IkB kinase
IL-1R	InterLeukin-1 Receptor
IRD	infantile Refsum disease
IRF	Interferon Regulatory Factor
iRhom2	inactive rhomboid 2
ISG	Interferon Stimulated Genes
JAK-STAT pathway	Janus Kinase-Signal Transducers and Activators of Transcription pathway
LBP	L-Bifunctional Protein
LD	Lipid Droplets
LDL-cholesterol	Low Density Lipoproteins cholesterol
LGP2	Laboratory of Genetics and Physiology 2
LRR	Leucine-Rich-Repeat
MAVS	Mitochondrial AntiViral Signalling
MDA5	Melanoma Differentiation Associated Gene 5
Mff	Mitochondrial fission factor
MyD88	Myeloid differentiation primary response 88
NAD^+	Nicotinamide adenine dinucleotide
NADH	Nicotinamide adenine dinucleotide Hydroxide
NALD	Neonatal adrenoleukodystrophy
NF-kB	Nuclear Factor kappa B
NO	Nitric oxide
O_2	Oxygen

PAMPs	Pathogen-Associated Molecular Patterns
PEX	peroxin
PI (4,5) P_2	Phosphatidylinositol 4,5-bisphosphate
PMPs	Peroxisomal Membrane Proteins
Pol III	Polymerase III
PRR	Pattern Recognition Receptor
PTS1	Peroxisome targeting signal 1
PTS2	Peroxisome targeting signal 2
RCDP	Rhizomelic chondrodysplasia syndrome
RIG-I	retinoic-acid-inducible protein 1
RLR	RIG-I like receptors
RNA	RiboNucleic Acid
ROS	Reactive Oxygen Species
SCP-X	Sterol Carrier Protein
SKL	Serine-Lysine-Leucine
STING	Stimulator of Interferon Genes
TBK1	Serine/threonine-protein kinase
TIR	Toll/IL-1R homology
TIRAP	TIR Domain Containing Adaptor Protein
TLR	Toll-like Receptor
TNF	Tumour Necrosis Factor
TRAF	Tumor Necrosis Factor Receptor-Associated Factors
TRAPb	Translocon-associated protein beta
UL82	Tegument protein pp71
US9	membrane glycoprotein US9
VAPB	Vesicle-Associated membrane Protein-associated protein B
VLCFA	Very Long Chain Fatty Acid
vMIA	viral Mitochondrial Inhibitor of Apoptosis
X-ALD	X-linked adrenoleukodystrophy
ZS	Zellweger syndrome

Index

List of figures

List of Tables

List of Equations

I. Introduction

I. Introduction

1.1. Peroxisomes

Peroxisomes are multifunctional, ubiquitous and dynamic organelles, which were only recognized as individual organelles in 1966 by *De Duve* and *Baudhuin*[1]. These small organelles (0.1 – 1.5µm in diameter) are spherical compartments delimited by a single phospholipid bilayer and composed by a fine granular matrix, containing crystalline inclusions of matrix enzymes. Peroxisomes can be found distributed throughout the cytoplasm in all eukaryotic cells and present remarkable plasticity, varying their size and shape in response to different stimuli[2,3].

Peroxisome biogenesis and degradation

Peroxisome biogenesis involves the generation of the peroxisome membrane and subsequent targeting and insertion of peroxisomal membrane proteins (PMPs) into the lipid bilayer, as well as the import of enzymes into the peroxisomal matrix[4]. The machinery that is involved in the peroxisome biogenesis is not totally understood and is rather complex. However, it is estimated to involve about 36 of the 85 genes that are known to encode peroxisomal proteins. The genes responsible for the biogenesis and maintenance of functional peroxisomes are designated as *Pex* genes and the proteins that are codified by them as peroxins (PEX)[5].

Peroxisomes can proliferate by growth and division of pre-existing peroxisomes or arise *de novo*[6]. The *de novo* model suggests the fusion of two pre-peroxisomal vesicles, each vesicle containing one of the two peroxisome-biogenesis initiating proteins PEX16 and PEX3, which are import receptors for PMPs. The import of PMPs to the fused-vesicles proceeds with their targeting to peroxisomes by the cytosolic chaperone PEX19[7]. The localization of PMPs at these vesicles converts peroxisomes into fully import-competent peroxisomes, allowing the import of matrix (lumen) proteins. Mature peroxisomes continue to import both PMPs and matrix proteins to maintain their functionality[8].

Until now, it was accepted that PEX16 and PEX3 targeted endoplasmic reticulum (ER) leading to the release of these vesicles from this organelle[4]. However, recently, *Sugiura et al.*[7] demonstrated that, in fibroblasts cells lacking PEX3, overexpressed PEX3 and endogenous PEX14 first target mitochondria to induce the production of pre-peroxisomal vesicles that maturated into fully

import-competent peroxisomes. They also suggest that for the rapid maturation of peroxisomes, it is necessary the fusion of pre-peroxisomal vesicles from mitochondria and ER, and that when pre-peroxisomal vesicles are formed exclusively in ER the maturation of peroxisomes is much slower[7]. Thus, both ER and mitochondria can contribute to the *de novo* formation of peroxisomes in mammalian cells[4].

The peroxisomal matrix proteins are synthesized on cytosolic ribosomes and post-translationally transported to the peroxisomes due to one of two peroxisomal targeting signals (PTS1 and PTS2). The PTS1 is a small C-terminal located peptide, frequently ending with the sequence SKL (serine-lysine-leucine), which is present in most peroxisomal matrix proteins. The PTS2 is a degenerated nonapeptide present at the N-terminal of just a few mammalian proteins. There is no clear knowledge about the recognition of these proteins and promotion of their translocation across the peroxisome membrane[9]. However, it is accepted that PTS1 and PTS2 matrix proteins are recognized by PEX5 and PEX7, respectively, in the cytoplasm[10]. PTS1 proteins are transported by oligomers of PEX5 into peroxisomes, where PEX14 functions as a convergent, initial docking site of the protein import machinery. For PTS2 proteins, PEX5 directly interacts with PEX7-PTS2 complex in the cytosol, transporting the complex to PEX14. PTS1 and PTS2 proteins are then released at the inner surface and/or inside of peroxisomes, downstream of PEX14 and upstream of PEX13. PEX5 and PEX7 induce the translocation of other constituents that make part of the translocation complex, which consist in the RING proteins: PEX2, PEX10 and PEX12. Both PEX5 and PEX7 finally shuttle back to the cytosol, where PEX1 and PEX6 catalyse their export[11].

Peroxisomes can rapidly increase in number by growth and division, which involves remodelling and expansion of the peroxisomal membrane, through the formation of tubular membrane extensions, which then constrict and divide into new peroxisomes (reviewed in [8]). For division to happen, PEX11β is described as being involved in peroxisome elongation and in recruitment of the fission adaptors mitochondrial fission factor (Mff) and fission factor 1 (Fis1), which in their turn recruit the dynamin like protein 1 (DLP1), contributing to the assembly of the peroxisomal division machinery (Figure 1)[12].

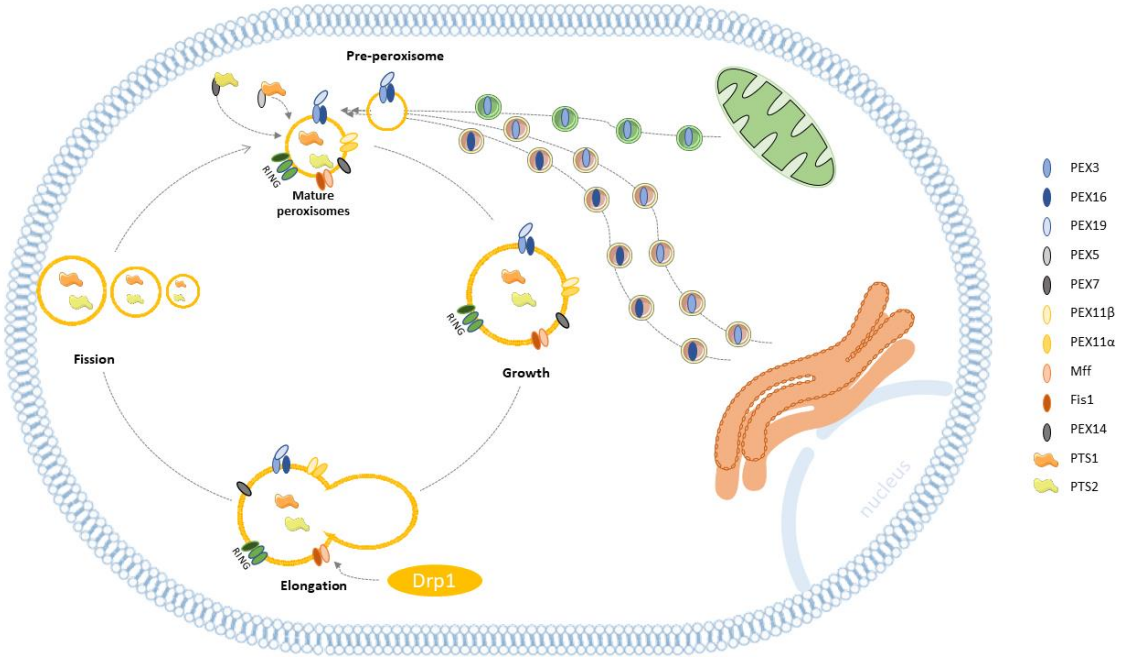

Figure 1. Schematic representation of peroxisome biogenesis (adapted from Kim P. 2017).

The estimated half-life time of mammalian peroxisomes is about 1.3 – 2.2 days, which requires the regulation of two main processes: the formation of new peroxisomes and the removal of old, abnormal and dysfunctional ones[13]. In fact, the peroxisome homeostasis is achieved via a tightly regulated interplay between peroxisome biogenesis and degradation via selective autophagy, which is commonly known as "pexophagy"[14]. Autophagy is the main form of cell degradation and there are three major types of autophagy: the chaperone-mediated autophagy, microautophagy and macroautophagy[15]. Pexophagy is a type of microautophagy where an obsolete, abnormal or dysfunctional peroxisome is sequestered into a specialized autophagosome[13].

Peroxisome metabolic functions

Peroxisomes are essential for the biosynthesis of cholesterol, dolichol, bile acids and most importantly in the β-oxidation of branched-chain and very long-chain fatty acids (VLCFA) and catabolism of polyamines and D-amino acids. Peroxisomes are also essential for the biosynthesis of the glycerophospholipids: plasmogens, which are highly abundant in the myelin sheath of neurons[6].

Reactive Oxygen Species Metabolism

One of the first functions to be described was the ability to reduce oxygen (O_2) to hydrogen peroxide (H_2O_2)[6]. In turn, the accumulation of H_2O_2, which is toxic to cells, must be compensated, therefore

H_2O_2 is decomposed by enzymes such as catalase, glutathione peroxidase and peroredoxin V (PMP20). The decomposition of H_2O_2 by catalase can be done catalytically (Equation 1) or peroxidatically (Equation 2) where the conversion of one molecule of H_2O_2 to two molecules of H_2O coupled with different hydrogen donors (AH_2), such as ethanol, methanol, formaldehyde, formate and nitrite, occurs. Besides that, peroxisomes can generate other reactive oxygen species (ROS) such as superoxide anions, nitric oxide (NO)[16]. These oxidants are toxic for cells but are also involved on redox signalling. With this, peroxisomal homeostasis is critical for proper cell function, manifested by the precise and efficient control of peroxisome number and functionality, tightly regulated in response to environmental changes[13].

Equation 1. Decomposition of H_2O_2 catalytically.

$$2H_2O_2 \rightarrow O_2 + 2H_2O$$

Equation 2. Reduction of H_2O_2 peroxidatically.

$$H_2O_2 + AH_2 \rightarrow A + 2H_2O$$

Ether Lipids Synthesis

Peroxisomes are responsible for the biosynthesis of lipids, such as glicerolipids, bile acids and steroids[17]. The synthesis of ether lipids in peroxisomes begins with the esterification of dihydroxyacetone phosphate (DHAP) with a long-chain fatty acid by the enzyme DHAP acyltransferase (DHAPAT), which replaces the fatty acid by a fatty acid-alcohol to form alkyl-DHAP by alkyl-glycerone phosphate synthase (AGPS)[4].

Fatty acid β-oxidation

Peroxisomes are responsible for β- and α-oxidation of fatty-acid. Although this process can be also performed by mitochondria, in mammals there are a set of fatty acids that are only oxidized by peroxisomes. These compounds include long-chain dicarboxylic and very long-chain monocarboxylic fatty acids, as well as long aliphatic carbon chain poorly soluble in water that are transformed in polar metabolites for their elimination. Besides that, polyunsaturated fatty acids are usually better and faster oxidized in peroxisomes than in mitochondria[18]. The peroxisomal β-oxidation is a four steps process: 1) dehydrogenation, 2) hydration, 3) dehydrogenation and 4) thyolisis[16,19]. The first step of peroxisomal β-oxidation is catalysed by acyl-CoA (ACOX). The second and third steps of peroxisomal β-oxidation are catalysed by two enzymes, the L- (LBP) and the D-

bifunctional proteins (DBP). The last enzymatic step is catalysed by a 3-ketoacyl-CoA thiolase. Additionally, in mammals the peroxisomal isoform of the sterol carrier protein (SCP-X) is an alternative thiolase that contribute to peroxisomal β-oxidation (Figure 2)[20]. Fatty acids with a methyl-group at the carbon 3 position cannot undergo by β-oxidation but must be α-oxidized first to produce the (n-1) fatty acid with the methyl-group at the 2 position. This process is described as confined only to peroxisomes[16].

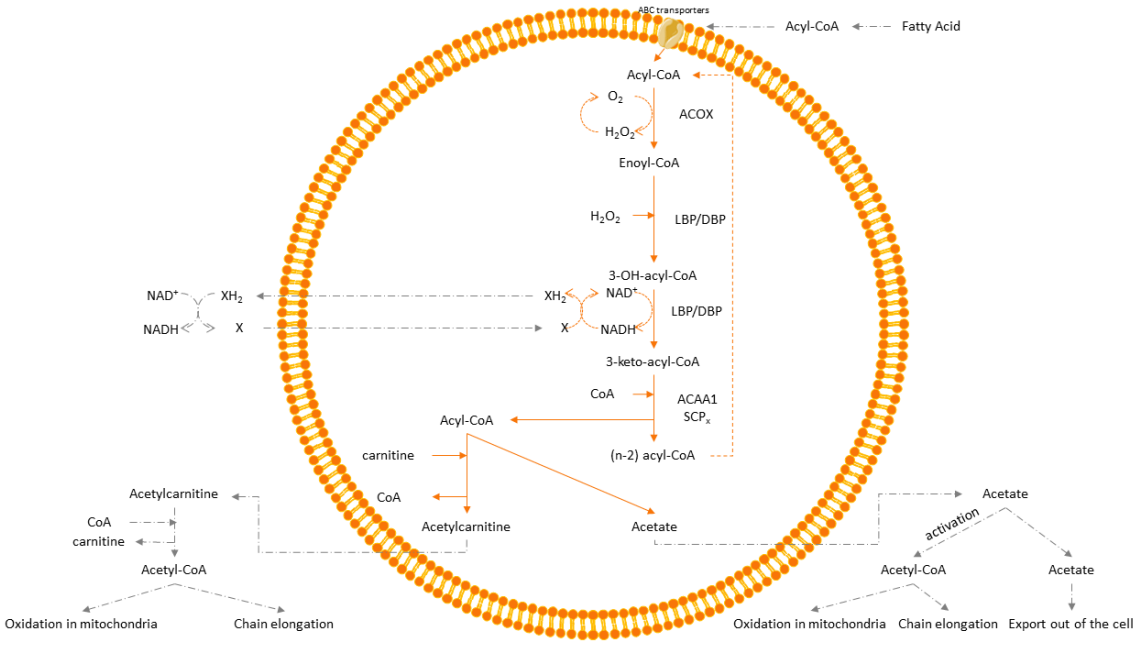

Figure 2. Schematic representation of Peroxisomal β-oxidation. In peroxisomes, molecular oxygen is the electron acceptor in the first step of β-oxidation, resulting in the formation of H_2O_2, which is reconverted into O_2 by catalase. The NADH generated in the third step of peroxisomal β-oxidation is reoxidized via NAD(H)-redox shuttle, involving the cytosolic and peroxisomal isoforms of lactate dehydrogenase. ACOX (acyl-CoA oxidases), LBP (L-bifunctional protein), DBP (D-bifunctional protein), ACAA1 (acetyl-CoA acyltransferase 1), SCPx (steril carrier protein x). (adapted from Wanders, RJA. and Waterham, HR. 2006).

Peroxisomes and other organelles

The communications between organelles include metabolic interactions, intracellular signalling, cellular maintenance, regulation of programmed cell death/cell survival or pathogen defence. This functional interplay can be established by vesicular transport, exchange of metabolites or signalling molecules, through diffusion or direct physical transport, which are mediated by specialized membrane contact sites. Besides, it is known that cytoskeleton and molecular motors are not the only organizers of cellular architecture and that membrane contacts can influence the positioning and motility of organelles. Organelle interactions depend also on the total number of organelles,

which are regulated by organelle biogenesis/formation, membrane dynamics and autophagic processes (reviewed in [21]) (Figure 3).

In fact, peroxisomes can form tubular membrane protrusions, which extend and retract and allows the interaction with other organelles. Peroxisomes play an essential role in intracellular transport through forming membrane contacts with lysosomes. This transport is mediated by lysosomal Synaptogamin VII binding to the lipid PI (4,5) P_2 on peroxisomal membrane. LDL-cholesterol (low density lipoproteins cholesterol) enhances such contacts and cholesterol is transported from lysosomes to peroxisomes[22].

Peroxisomes interact also with lipid droplets (LD), specialized organelles involved in storage neutral lipids such as triacylglycerols and sterol esters for energy and membrane homeostasis. Peroxisomes are frequently found in close association with LD[23], which may be associated with the supply of fatty acids by lipolysis in LD with peroxisomal VLCFA β-oxidation. Besides, the exchange of lipids between these organelles may serve membrane replenishment or storage in lipid droplets[21].

Peroxisomes establish interactions with ER, cooperating in several pathways, such as the production of ether-phospholipids, as plasmogens and polyunsaturated fatty acids, which start to be produce at peroxisomes but their synthesis finishes at ER[24]. In mammals it was also described that, besides the metabolic cooperation, the ER can play a role in *de novo* generation of peroxisomes, as previously indicated. Moreover, the ER provides phospholipids for the formation, as well as elongation of the peroxisomal membrane. After *Novikoff* and *Shin*[23] reported the proximity between peroxisomes and ER, several other reports have emerged showing contact sites between the ER and peroxisomes, and these are associated with the biogenesis of peroxisomes, as derivatives of the ER, and to the exchange of metabolites for biochemical pathways[25]. Also recent studies[24,26] have shown that ACBD5 and ACBD4 isoform 2 act as tethers between peroxisomes and ER. These are members of the acyl-CoA binding protein (ACBP) family which are characterized by an acyl-CoA binding domain (ACBD), which allows their binding to lipids, namely acyl-CoA esters, intermediates of β-oxidation[27]. Both interact with vesicle-associated membrane protein-associated protein B (VAPB), an ER protein that functions as an adaptor in inter-organellar lipid exchange and membrane tethering. Although the role of the ACBD4 isoform 2 in peroxisomes-ER interaction is not fully understood, it was demonstrated that the interaction between peroxisomes and ER depends of ACBD5-VAPB interaction[28]. ACBD5 was reported to affect peroxisomes motility and peroxisomes membrane elongation, likely because of the reduced transfer of membrane lipids. In

fact, in the absence of ACBD5-VAPB interaction, the peroxisomal membrane expansion is reduced, suggesting that the lipid flow from the ER to peroxisomes is required for peroxisomal membrane growth. In addition, the movement of peroxisomes was increased[26]. Furthermore, it was describes that patients that possess ACBD5 deletion present increased levels of VLCFA but a reduced import to peroxisomes, what suggest that ACBD5 can have a role on the sequestration of VLCFA and in their import to peroxisomes[29].

The interactions between mitochondria and peroxisomes are another example of essential metabolical interactions. These two organelles cooperate in the cellular lipid metabolism, in particular the breakdown of fatty acids, via their organelle-specific β-oxidation pathways. Both organelles are crucial for cellular redox homeostasis, and disturbances in peroxisomal lipid and ROS metabolism have an impact on the mitochondria redox balance, which leads to an increase of mitochondrial stress, and consequently in the activation of mitochondrial stress pathways[30]. Besides, peroxisomes and mitochondria share proteins of their division machinery, the dynamin-related GTPase Drp1/DLP1 and the membrane adaptor proteins Fis1 and Mff[4,21]. Mitochondria and peroxisomes are both important signalling nodes in the cell and have cooperative functions in anti-viral and redox signalling[31].

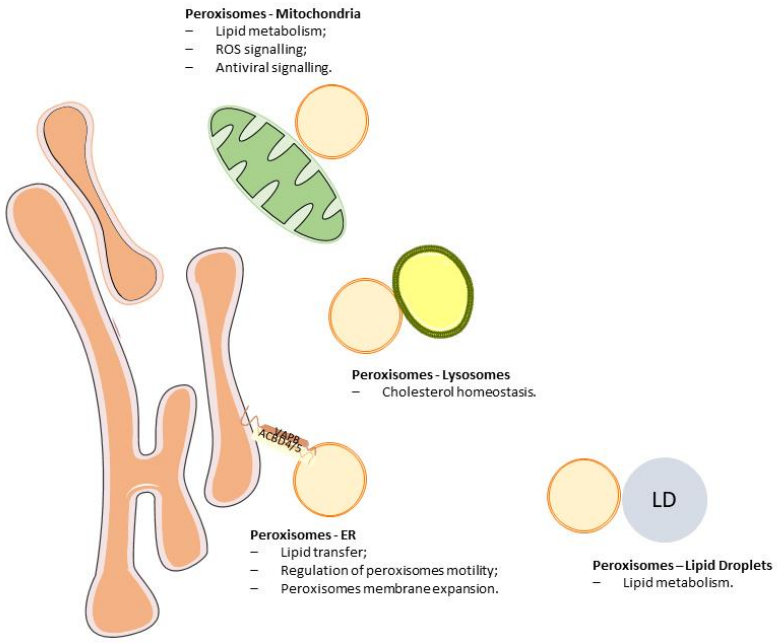

Figure 3. Schematic representation of interactions between peroxisomes and other organelles in mammals. (adapted from Islinger, M. et al. Histochem 2012.)

Peroxisomal disorders

Disorders that involve peroxisomes are normally related with enzymes of VLCFA β-oxidation, isoprenoid biosynthesis, ether-phospholipids synthesis, glyoxylate detoxification, phytanic acid α-oxidation, L-pipecolate degradation, glutaryl-CoA metabolism, hydrogen peroxide metabolism and deficiency on peroxisomal biogenesis protein[32].

Diseases associated to peroxisomal biogenesis are inherited in an autosomal-recessive manner and they differ on the severity of symptoms. These include two syndromes, the Zellweger syndrome (ZS) and the Rhizomelic chondrodysplasia syndrome (RCDP) spectrum, described for mutations in *Pex1, Pex2, Pex3, Pex5, Pex6, Pex10, Pex12, Pex13, Pex14, Pex16, Pex19* and for mutations in *Pex7*, respectively[33]. The first comprises the Zellweger syndrome (ZS), neonatal adrenoleukodystrophy (NALD) and infantile Refsum disease (IRD). These are characterized by an accumulation of VLCFA, phytanic acid and bile acid intermediates. The infants live only a few months and show liver involvement, hypotonia, seizures, feeding difficulties and apnea. The second spectrum is characterized by one or two years of survival and present dysmorphism with disturbed endochondral bone formation and severe psychomotor delay[34].

Diseases with mutations on the enzymes involved in different peroxisomal metabolic functions are inherited as autosomal recessive traits except for X-linked adrenoleukodystrophy (X-ALD). X-ALD is the most common single peroxisomal disease with an incidence of 1 per 20000 males, having about 50% of heterozygous ALD woman develop a syndrome in middle age due to random inactivation of the X chromosome. The X-ALD have a defective ABCD1 gene, which encodes a peroxisomal membrane protein responsible for mobilizing VLCFA into the peroxisomes for degradation leading to an accumulation of VLCFA, primarily in white matter and adrenocortical cells[32,33].

1.2. Cellular antiviral response

The innate immune response in mammals initiate when microorganisms are recognized by specialized receptors, designated as pattern recognition receptors (PRR) (reviewed in [35]). After the recognition of pathogen-associated molecular patterns (PAMPs), PRRs initiate downstream signalling cascades that culminate with the expression of cytokines such as interleukin-1, tumour necrosis factor (TNF), interferon stimulated genes (ISG) and type I and III interferon (IFNs)[36].

RIG-Like Receptors (RLR)

The cytosolic RLRs include retinoic-acid-inducible protein 1 (RIG-I), melanoma differentiation-associated protein 5 (MDA5) and laboratory of genetics and physiology 2 (LGP2). They present a central ATPase containing DExD/H box helicase domain and a C-terminal regulatory domains (CTDs)[37]. RIG-I and MDA5 contain two CARD domains that mediate the downstream signalling, while LGP2 lacks these domains.

Upon viral infection, RIG-I and MDA5 recognize viral RNA, which induces binding to the mitochondrial antiviral signalling protein (MAVS)[38]. At peroxisomes and mitochondria MAVS is the adaptor protein in the RLR pathway and contains a CARD domain at its N-terminal, a central proline-rich region and a C-terminal transmembrane domain. The interaction between its CARD domain and RIG/MDA5 CARD domains induces MAVS oligomerization into prion-like aggregates, which allows a large amplification of the activation signal to other MAVS that were not directly activated[39]. MAVS activation recruits the tumour necrosis factor receptor-associated factor (TRAF) 2/6, which are necessary for the activation of TRAF family member associated NF-kB activator-binding kinase 1 (TBK1) protein and the IkB (IKK) complex activation. TBK1/IKKε and IKK complex activation induce the phosphorylation of the interferons regulator factors (IRF) IRF3/IRF7, as well as NF-kB, respectively[40,41]. IRF3/7 and NF-kB are then translocated to the nucleus, together with ATF2, c-Jun and the transcription co-activator CREB-binding protein to activate the expression of interferons and pro-inflammatory gene expressions[42]. Once secreted, IFNs bind to specific cell surface receptors and activate the JAK-STAT pathway that will lead to the activation of transcription factor STAT1, STAT2 and IRF9 originating the IFN-stimulated gene factors (ISGF3). This will be translocated to the nucleus and will coordinate the transcription of IFNs, chemokines and ISGs[43].

Interestingly, the presence of MAVS at both organelles induces different but complementing responses: peroxisomal MAVS induces a rapid but short-termed expression of ISGs while mitochondrial MAVS induces a delayed but long lasting expression of IFNs and ISGs[31]. While it is still controversial, the same group have showed that in specific cells, peroxisomal MAVS induces the expression of type III IFNs, whereas mitochondrial MAVS only induces the expression of type I IFNs[44].

Cytosolic DNA sensors

There is also a specific set of cytosolic PRRs that recognizes viral DNA, such as cyclic guanosine monophosphate–adenosine monophosphate (cGAMP) synthase (cGAS), DNA-dependent RNA polymerase III (Pol III), absent in melanoma 2 (AIM2), IFN-inducible protein 16 (IFI16), and the DNA-dependent activator of IFN-regulatory factors (DAI)[35]. The cyclic guanosine monophosphate-adenosine monophosphate (cGAMP) synthase (cGAS), binds to the adaptor protein stimulator of interferon genes (STING). Upon viral infection, viral DNA binding to cGAS catalyses the production of cGAMP, which in turn activates STING. STING activation involves the dimerization of this protein at ER membrane and consequent translocation to Golgi and perinuclear regions. This results in the activation of the transcription factors IRF3 and NF-kB, through TBK1-IKKε and IKKα and IKKβ respectively, and inducing consequently the expression of IFNs, ISGs and cytokines in a STING dependent manner[45].

Toll Like Receptors (TLRs)

TLR are normally the first responders to infection signals. These are type I integral membrane glycoproteins characterized by the extracellular domains containing varying numbers of leucine-rich-repeat (LRR) motifs and a cytoplasmic signalling domain homologous to the interleukin 1 receptor (IL-1R), termed Toll/IL-1R homology (TIR) domain[46]. Based on their primary sequences, TLRs can be divided in subfamilies according to the type of PAMPs they recognize. Upon infection, the recognition of PAMPs leads to the dimerization of TIR domains, recruiting their adaptors, TIRAP or MyD88, depending on the TLR that is activated. This initiates the formation of a large helical oligomer named the mydossome. This complex mediates the activation of inflammatory transcription factors, such as NF-kB and IRF, leading to their translocation to the nucleus and promoting the expression of IFNs and other inflammatory mediators (reviewed in [47]).

1.3. Human Cytomegalovirus (HCMV)

HCMV is a prevalent virus, that after a primary infection can induce a lifelong latent infection. However, in an immunocompromised individual can lead to serious and self-limiting disease, particularly in transplant recipients, HIV infected and new-borns of infected mothers[48,49].

Virus Structure

HCMV or human herpesvirus 5 is a β-herpesvirus subfamily of *Herpesviridae* family that possesses a dsDNA genome consisting in 235000 base pairs which encode a large number of open reading frames[50]. As for all *Hespesviridae*, the genome is packed within an icosahedral capsid, which has a dense proteinaceous matrix named tegument, which in turn is surrounded by a lipid envelope extensively coated with viral glycoproteins (Figure 4).

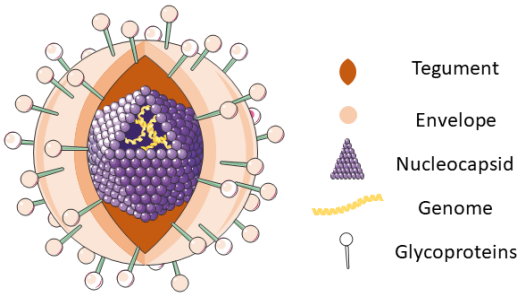

Figure 4. Schematic representation of HCMV structure (adapted from ViralZone:www.expasy.org/viralzone, SIB Swiss Institute of Bioinformatics).

Life cycle

Upon infection, receptors present in cell membrane bind to HCMV glycoproteins located in the virion envelope inducing endocytose or direct diffusion and releasing the viral capsid into the cytosol to be transported to the nucleus. Once in the nucleus, HCMV genome is replicated and transcribed leading to the release of viral RNA into the cytoplasm, where it will be translated[49,51].

HCMV gene expression and genome replication is a regulated process characterized by the sequential expression of differential classes of viral genes. Immediate early genes, expressed within hours (hrs) after infection, regulate intrinsic and innate host cell responses to infection and initiate transcription of viral genes indispensable for genome replication[52]. Early genes contribute to viral

DNA replication and packaging and regulate host cell functions to facilitate viral replication. Early viral gene products provide important functions necessary for genome replication, including among others the viral DNA polymerase[53]. Finally, the late viral genes encode structural proteins of the outer tegument layer and the envelope required for assembly of the infectious virion[49]. These lead to the capsid assembly and exit from the nucleus. In the cytosol, the capsid associates with tegument proteins before being transported to the viral assembly complexes, which contains machinery components of ER, Golgi apparatus that will be necessary for the formation of the viral envelope. The new virion particles are then released of the cell by exocytosis[54](Figure 5).

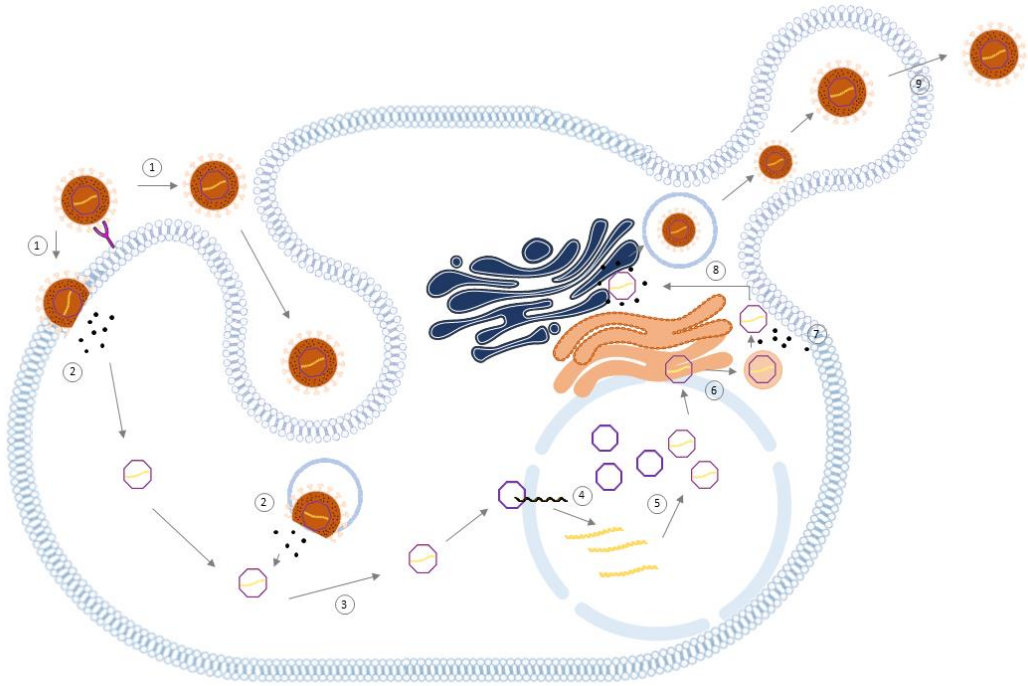

Figure 5. Schematic representation of human cytomegalovirus cycle infection. (1) Infectious particles enter the cell through interaction with cellular receptors or by endocytose. (2) Nucleocapsid and tegument particles are delivered to the cytosol. (3) The nucleocapsid travels to the nucleus, where the genome is delivered and circularized. (4) Tegument proteins regulate host cell responses and initiate the temporal cascade of the expression of viral genes and posterior viral genome replication. (5)(6) Then, capsid assembly is initiated in the nucleus, followed by nuclear egress to the cytosol. (7) Capsid associates with tegument proteins in the cytosol and are trafficked to the viral assembly complex that contains components of the ER and Golgi apparatus machinery. (8) The capsids bud into intracellular vesicles at the assembly complex. (9) Enveloped infectious particles are released along with non-infectious dense bodies (adapted from Beltran, PMJ. et al. 2014.).

HCMV evasion from the cellular antiviral response

HCMV has developed distinct strategies to counteract the cellular antiviral defences. Since HCMV is an dsDNA virus one of the main pathways activated is the STING-dependent antiviral response. It has been described that UL82, a HCMV tegument protein inhibits the STING signalling pathway. UL82 interacts with STING and iRhom2, disrupting the complex STING-iRhom2-TRAPβ and inhibiting the trafficking of STING, from the ER to the perinuclear region[55]. Besides, a recent study showed that the HCMV IE86 protein can impair STING-induced antiviral response by down-regulating the protein levels of STING, as well as through the inhibition of the transcription factors required for IFN-β promoter activation[56].

Besides targeting the STING-dependent antiviral signalling, it has been reported that HCMV also has means to subvert the RLR antiviral response. HCMV US9 glycoprotein was reported to target the MAVS-mediated signalling, impairing IFN-β production[57]. Additionally, the viral mitochondria-localized inhibitor of apoptosis (vMIA), a product of HCMV UL37 gene, has also been associated to the inhibition of MAVS downstream signalling, both at peroxisomes and mitochondria. This protein was known to be required for viral replication, as well as for the inhibition of apoptosis induced by diverse stimuli[58]. Although this protein does not share a sequence homology with any BCL-2 family member, it binds and inactivates Bax, but not Bak, to prevent mitochondrial outer membrane permeabilization[59]. Also vMIA induces the release of ER Ca^{2+} stores into the cytosol and triggers fragmentation of the mitochondria, which is necessary for the inhibition of the mitochondria-dependent antiviral signalling pathway[58]. Moreover, it was reported that mitochondrial fragmentation disrupts the interaction STING-MAVS, also required for an efficient cellular antiviral response. At peroxisomes, vMIA was shown to interact with MAVS and also inhibit the peroxisomal-dependent RLR signalling, however via a seemingly distinct mechanism, as peroxisomal fragmentation is not required[60].

II. Aims

II. Aims

The involvement of the peroxisomes as signalling platforms for the establishment of the cellular antiviral response raises the question whether one or more peroxisomal metabolic functions may be specifically relevant for this mechanism. On the other hand, the crucial interplay between peroxisomes and the ER may also play a role on the establishment of the peroxisome-dependent antiviral signalling.

The main propose of this work was to further unravel the mechanisms underlaying the peroxisome-dependent antiviral response, more specifically by trying to understand the relevance of peroxisome metabolism and interaction with the ER. Also, to study the role of ACBD5 on the peroxisomal-dependent antiviral signalling and to understand the effect of the interaction between peroxisomes and ER in the cellular antiviral response. Moreover, we investigate the peroxisomal metabolism upon activation of peroxisomal-dependent antiviral signalling.

To achieve these objectives the following aims were proposed:

1. Analyse peroxisome metabolism upon RLR signalling activation.
    a. Analyse the expression of different peroxisome proteins on stimulated cells.
    b. Apply FTIR assays to analyse the metabolic profile of stimulated cells.
2. Study the role of ACBD5 on the peroxisomal-dependent antiviral signalling.
    a. Analyse the MAVS signalling activation on ACBD5 KO cells.

III. Materials and Methods

III. Materials and Methods

3.1. Materials

Cell lines

HepG2	Liver hepatocellular carcinoma cells
MEFs	Mouse Embryonic Fibroblasts
MEFs ACBD5 knockout	Mouse Embryonic Fibroblasts with absence of ACBD5 protein
MEFs MAVS-PEX	Mouse Embryonic Fibroblasts with MAVS only at peroxisomes
HEK 293T	Human Embryonic Kidney 293 cells that expresses a mutant version of the SV40 large T antigen

Cell culture solutions

Dulbecco's Modified Eagle Medium (DMEM) High Glucose w/L-Glutamine w/o Sodium Pyruvate	Gibco
Fetal Bovine Serum (FBS), qualified, E.U.-approved, South America origin	Gibco
Penicillin/Streptomycin	Gibco
Dulbecco's Phosphate Buffered Saline w/o Calcium w/o Magnesium	Gibco
Trypsin-EDTA 1x in PBS w/o Calcium w/o Magnesium w/o Phenol Red	Gibco
Polyethylenimine (PEI)	Sigma-Aldrich
Lipofectamine 3000	Invitrogen
P3000	Invitrogen
Opti-Mem Reduced-Serum Medium (1x)	Gibco

Bacterial strains

Escherichia coli	DH5α

Bacterial Media

Table 1. List of solutions for bacterial media.

LB media	2,5g NaCl	ACROS
	10g Lysogeny Broth	Fisher Scientific
	1L ddH_2O	
Agar	17,5g Agar	FORMEDIUM
	2,52g NaCl	ACROS
	500mL ddH_2O	

Antibiotics

Ampicillin (Amp)	Sigma-Aldrich
Kanamycin (Kan)	Sigma-Aldrich

Viruses

Sendai virus	Given by Dr. Jonathan Kagan, Harvard School University

Plasmids

Table 2. List of plasmids.

Plasmid	**Tag**	**Antibiotic Resistance**	**Company**
pEGFP-C1-RIG-I-CARD	GFP	Kan	Given by Dr. Friedmann Weber, Justus Liebig University
pcDNA3.1-vMIA-myc	Myc	Amp	Given by Dr. Goldmacher, ImuunoGen Inc.

Primers and Oligonucleotides

Table 3. List of PCR primers.

PCR primers			**Manufactures**
IRF1	IRF1 mouse	Forward 5’ GGTCAGGATTGGATATGGA 3’ Reverse 5’ AGTGGTGCTATCTGGTATAATGT 3’	Eurofins
GAPDH	GAPDH mouse	Forward 5’ AGTATGTCGTGGATCTA 3’ Reverse 5’ CAATCTTGAGTGAGTTGTC 3’	Eurofins
Acox1	Acox1 mouse	Forward 5’ AGTTAATCACGCACATCT 3’ Reverse 5’ CCTCATCTTCTTCACCAT 3’	Eurofins
Catalase	Catalase mouse	Forward 5’ TTATCCATAGCCAGAAGAGAA 3’ Reverse 5’ TCGGTCACTGAACAAGAA 3’	Eurofins
Pex14	Pex14 mouse	Forward 5’ GCCACCACATCAACCAACT 3’ Reverse 5’ GGGAAGGAGGGAACTGTC 3’	Eurofins

Transfection Reagents

Polyethylenimine (PEI)	Sigma-Aldrich
Lipofectamine 3000	Invitrogen
P3000	Invitrogen

Markers and Loading Dyes

Table 4. List of markers and loading dyes for SDS and agarose gel.

GRS Protein Marker Multicolour Tris-Glicine		Grisp
6x Laemmli Buffer	350mM Tris pH 6,80	Thermo Fisher
	10mM Sodium Dodecyl Sulfate (SDS)	Fisher Scientific
	60mM dithiothreitol (DTT)	NewEngland Biolabs
	0,06% Bromophenol Blue	Sigma-Aldrich
O´Gene Ruler DNA Ladder Mix		Thermo Fisher
6x Orange DNA Loading Dye		Thermo Fisher

Kits

QIAGEN® Plasmid Mini, Midi and Maxi Kits	QIAGEN®

Antibodies

Table 5. List of antibodies.

Primary	Species	Production	Dilution		Company
			WB	IMF	
myc	Mouse	Polyclonal		1:2000	Cell Signalling
GFP	Chicken	Polyclonal		1:500	Acris
Acox1	Rabbit	Polyclonal	1:10000		Given by Dr. Takashi Hochimoto, Shinshu University
α/β tubulin	Rabbit	Polyclonal	1:2000		Cell Signaling
Pex14	Rabbit	Polyclonal	1:20000		Dako
Catalase	Rabbit	Polyclonal	1:10000		Given by Dr. Alfred Voelkl, University of Heidelberg

Solutions and Buffers

Table 6. List of solutions and buffers.

Solutions	Reagents	Company
Ammonium Persulfact (APS)	0.2% APS	Sigma-Aldrich
Blotting Buffer	48 mM Tris Base	Fisher Scientific
	39 mM Glycine	Fisher Scientific
	0.04% SDS	Fisher Scientific
	20% MeOH	Merck Milipore
Foy 305		Schwarz Pharma
Freezing Medium	DMEM	Gibco
	20% FBS	Gibco
	10% DMSO	Sigma-Aldrich
Hidrocloric Acid (HCL)		Merck Millipore
Mowiol	¾ Mowiol	Apply Chem
	¼ n-propyl-Gallat	Sigma-Aldrich
Milk		Nestle
Paraformaldehyde (PFA)		Sigma-Aldrich
Phenylmethanesulfonyl		Sigma-Aldrich

Fluoride (PMSF)		
Ponceau Solution	0.1% *Ponceau*	ROTH
	0.5% Acetic Acid	Merck Millipore
1x TVBE	1mM NaHCO3	Sigma-Aldrich
	1mM EDTA	Sigma-Aldrich
	0.1% Triton X-100	Sigma-Aldrich
10x TBS-T	100 mM Tris Base	Fisher Scientific
	1.5 M NaCl	ACROS
	0.05% Tween 20	Sigma-Aldrich
50x TAE	0.04 M Tris-HCl	Fisher Scientific
	0.02 M Acetic-acid	Merck Millipore
	1 mM EDTA	Sigma-Aldrich
10x Transfer Buffer	48 mM Tris	Fisher Scientific
	39 mM Glycine	Fisher Scientific
	0.04% SDS	Fisher Scientific
	20% methanol	Merck Millipore
10x SDS – Running buffer	250 mM Tris	Fisher Scientific
	1.9 M Glycine	Fisher Scientific
	20% SDS	Fisher Scientific
NaOH		ROTH
Bovine Serum Albumin (BSA)		NZYTech
Aprotinine (Trasylol)		Bayer
10x PBS	1.369 M NaCl	ACROS
	0.0268 M KCl	Sigma-Aldrich
	80 mM Na_2HPO_4	Sigma-Aldrich
	0.0147 M KH_2PO_4	Sigma-Aldrich

Databases and Softwares

- AxioVision Software, Zeiss;
- Zen Software, Black Edition, Zeiss;
- Excel, Microsoft;
- Graphpad, Prism 7;

- Image Studio Software for Odyssey;
- Quantity One 1-D Analysis Software, Bio-Rad;
- National Centre for Biotechnology Information (NCBI);

Equipment

- CO_2 incubator MCO-17AIC, Sanyo;
- Vertical Laminar Flow Hood HERASafe, Heraeus;
- Water Bath VW36, VWR;
- Pipettes Eppendorf Research, Eppendorf;
- My Cycler Thermal Cycler, BioRad;
- The Unscrambler X, CAMO;
- UV-3100 PC Spectrophotometer,
- VWR DeNovix DS-11 Software, DeNovix;
- Vaccum gas pump, VWR;
- 7500 Real-Time PCR System, Applied Biosystems.
- AxioImager Z1 Zeiss Microscope

3.2. Methods

Cell culture

Cell lines maintenance

To perform the current work, the cell lines used were hepatocellular carcinoma (HepG2), Mouse Embryonic Fibroblasts (MEFs) wild type (WT), MEFs ACBD5 Knock-out (KO) and MEFs MAVS-PEX. HepG2 were obtained from American Type Culture Collection, HB-8065. The MEFs WT and MEFs ACBD5 KO were kindly provided by Dr. Markus Islinger from University of Heidelberg. The MEFs MAVS-PEX were kindly provided by Dr. Kagan from Harvard Medical School.

All the cell lines were routinely cultured and split twice a week in 10Øcm dishes when reached approximately 80% confluency, with high glucose DMEM (8.4mL/L, Gibco) supplemented with 10% FBS and 1% Penicillin/Streptomycin (Pen/Strep, Gibco). The cells were maintained in culture at 37°C and 5% CO_2. To split cells, they were washed one time with 1x PBS (Gibco) and then incubated with 1x trypsin-EDTA, after which were resuspended with complete DMEM and centrifuged at 1000 rpm, 3 minutes. The supernatant was discarded, and the pellet was resuspended in 10 mL of complete DMEM. From this, the cells were either used to perform experimental procedures and/or seeded in a 1:10 dilution and kept in a 37°C, 5% CO_2 incubator.

Cell storage, freezing and thawing

Stocks from cells were made from 80-90% confluent cells resuspended in DMEM with 10%FBS and 10%DMSO and were kept in cryovials aliquots of 1.5mL. Stocks were frozen in -80°C before being placed in the liquid nitrogen tank for cryopreservation.

For thawing and use it, frozen cells were thawed through resuspension in complete DMEM and seeded in a 10Øcm culture dishes. After cell adhesion, approximately 6 hours (hrs), the medium was replaced to eliminate the DMSO that is toxic for cells at room temperature.

Transient Mammalian Transfection Methods

Polyethylamine (PEI)

Polyethylemine (PEI, Sigma-Aldrich) is a stable cationic polymer that allows DNA condensation into positively charged particles that bind to anionic cell surfaces. This DNA-PEI complex is endocytosed by the cells and DNA is then released into the cytoplasm[61].

To perform the transfection in 6-well or 10Øcm plates, 5 and 20 µg of DNA, respectively, were diluted in DMEM w/o FBS w/o Pen/Strep. Then 25 and 100 µL of PEI was added to the diluted DNA (1:5 DNA:PEI ratio), who was vortexed for 10 seconds and incubated at room temperature for 15 minutes. Meanwhile, the cells were washed 3 times with high glucose DMEM with 10% FBS. The PEI-DNA complex formed was added dropwise to cells in complete DMEM. Cells incubated in 37°C 5% CO_2 for the desire time before being collected and processed. This procedure was used to transfect vMIA-myc and GFP-RIG-I-CARD into HepG2 cells.

Lipofectamine 3000

The lipofectamine (Invitrogen) transfection method was used on MEFs WT, MEFs ACBD5 KO and MEFs MAVS-PEX cells. In this cationic lipid-mediated method, the negatively charged DNA binds spontaneously to the positively charged liposomes, forming DNA cationic lipid reagent complexes. To perform this transfection, the Lipofectamine 3000 (Invitrogen) was diluted on Opti-MEM (Gibco) a reduced serum media on a 1:30 proportion. Also, the DNA was diluted on Opti-MEM 3µg/90µL and P3000 (Invitrogen) was added to the diluted DNA slowly. The DNA/P3000 complex was added to the diluted Lipofectamine 3000 and the solution was incubated for 5 minutes at room temperature. Before adding the mixture dropwise to the cells, growth media was changed to fresh complete media. The transfection timepoints were the same as indicated previously.

Transforming competent cells

For bacterial transformation, 5ng of pEGFP-C1-RIG-I-CARD and pcDNA3.1-vMIA-myc were added to 50 µL of *Escherichia coli* DH5α cells. After a 30 minutes incubation on ice, the cells were subjected to a heat shock for 20 seconds at 42°C on Thermoblock (Eppendorf). The tubes were then placed on ice for 2 minutes before adding 950µL of pre-warmed LB medium. This was followed by an incubation at 37°C for 1 hour at 225 rpm. 100µL from each transformation was spread on antibiotic-selective plates, which were incubated overnight at 37°C. Afterwards, colonies were picked and

inoculated in 3mL of LB medium with antibiotic for 16 hours at 37°C with shaking at 225 rpm. Cellular suspension was then added to 100mL of medium with antibiotics. To finally obtain the plasmids, they were purified following the QIAGEN® Plasmid Midi Kit protocol and the final concentration was measured on nanodrop (DeNovix).

Fourier Transformed Infrared Spectroscopy (FTIR) assay

Cell preparation for FTIR

After transfection, cells from 10Øcm dish were washed with 4 mL of 1x PBS and trypsinized with 2 mL of trypsin-EDTA 1x. After trypsinization, cells were resuspended in 4 mL of complete DMEM medium and centrifuged at 1000 rpm for 3 minutes. The supernatant was discarded, and the pellet was resuspended in 10 mL of complete DMEM.

Then cells were divided into 10 tubes of 1.5 mL with $1x10^6$ cells each and were centrifuged at 1000 rpm for 3 minutes. After that, the supernatant was discarded and the pellet was washed in 1 mL of 1x PBS, and again centrifuged at 1000 rpm for 3 minutes. The pellet was kept on ice until FTIR analysis.

Spectral Imaging

All the spectra were acquired on a FTIR spectrometer ALPHA II (Bruker Corporation, Massachusetts, USA) controlled by OPUS software (Bruker Corporation, Massachusetts, USA). FTIR spectra were obtained in the wavenumber range 600-4000 cm^{-1}, with a resolution of 8 cm^{-1} and 64 co-added scans. Between each measurement a background spectra was acquired with the empty crystal. The room conditions were kept constant at 35% of relative humidity and 23°C.

Multivariate analysis

The FTIR spectra were analysed by Unscrambler® X software, version 10.5.1 from CAMO software. All spectra were area-normalized to allow intra- and inter-group comparisons. To enhance the biochemical differences between samples, 2nd derivative analysis was performed, using *Savitzky-Golay* algorithm with 3 smoothing points. A Principal Component Analysis (PCA), using 7 principal components, was carried from where the scores and loadings plots were analysed.

Viral infection

HEK 293T cells were infected with Sendai virus (SeV) with 0.0001u/cell from stocks at 4000u/mL diluted in serum and antibiotic free media. After removing the growth media, virus dilution was added to the plates. After incubating cells for 1 hour at 37°C, the same virus dilution was added to the plates. After incubating cells for 1 hour at 37°C, the same virus dilution volume of growth media containing 20% of FBS was added to the cells. The cells were then processed for protein extraction and blotting protocol that will be described below.

Western Blot

Protein extraction

For protein extraction, cells were washed twice with 1x PBS and lysis buffer (25 mM Tris-HCl pH8, 50 mM NaCl, 0.5% sodium deoxycholate monohydrate and 1.5 mM Triton X-100) supplemented with the proteases inhibitors Foy 305 (Camostat Mesilat, Scharz Pharma), aprotinin (Bayer) and PMSF (Phenylmethylsulfonyl fluoride, Sigma) was added. Cells were scrapped and collect to an adequate tube and resuspended with a 20g syringe and left for an overhead rotation for 30 minutes. After a centrifugation at 13000rpm for 15 minutes, nucleic acids and other debris were pelleted, and the protein were obtained in the supernatant that was kept at -20°C.

Protein quantification

The quantification of the extracted protein was made measuring the absorbances of each sample, using the Bradford method. For that, each sample was diluted in the TVBE buffer (1mM $NaHCO_3$, 1mM EDTA, 0.1% Triton X-100) in a proportion 1:200 or in sodium hydroxide (0.1M NaOH, ROTH) in a proportion of 1:20. As a comparation, the diverse dilutions of known concentrations of BSA were performed. The Bradford reagent was diluted 1:5 and was added to each of diluted samples. The absorbance at 595 nm was measured and a standard curve was draw on Microsoft Excel program. The samples concentration was obtained.

SDS-PAGE and transfer

The desired amount of protein, 5-80µg, was mixed in 5x loading buffer (350mM Tris, 10 mM SDS, 60mM DTT, 0.06% bromophenol blue and glycerol). Samples were then denaturated for 5 minutes at 95°C before being loaded in 12% polyacrylamide resolving and 4% stacking gel alongside with a pre-stained protein marker (GRS Protein Marker Multicolour Tris-Glicine, Grisp). The

electrophoresis chamber was filled with 1x Running buffer (25 mM Tris, 0.2M Glycine, 20% SDS) and the electrophorese was performed at 50V until samples reached the resolving gel being then changed to 100V. Then, proteins were electro-transferred onto a PVDF/nitrocellulose membrane in a semidry system (BioRad), during 45 minutes at 12V.

Immunoblotting

Membranes were blocked with 5% milk in 1xPBS or 1xTBS-T for about 1 hour. Primary antibodies incubation was performed for 1 to 3 hrs at room temperature, or overnight at 4°C, while secondary antibodies incubated for 1 hour at room temperature. Between blocking and antibodies incubation, membranes were washed 3 times for 5 minutes with 1xTBS-T.

Depending on the secondary antibody used, membranes were analysed by chemiluminescence or fluorescence detection methods. For chemiluminescence detection, the 2 substrates for horseradish peroxidase (HRP), a stable peroxidase solution and an enhanced luminol solution, were mixed in a 1:1 ratio. The conjugation of these two substrates in the presence of HRP induces chemical reaction which generates luminescence. Hence, membranes were incubated for 1 to 5 minutes with the mixed substrates and the Chemidoc Alliance (UVITEC) was used to detect proteins. For fluorescence detection, secondary antibodies are coupled with a fluorescent probe and detection was directly done on Odyssey System Imaging (LI-COR SYSTEM). The quantification of each band was made using the Quantity One software (BioRad), using α/β tubulin as reference.

Immunofluorescence

To perform the immunofluorescence assay, 12Ø or 18Ømm coverslips were added to the plates before seeding cells. After the transfection assays, the coverslips were taken off and were washed with 1xPBS at room temperature. Then, the coverslips were fixed with 4% paraformaldehyde (PFA, Sigma-Aldrich) for 10-20 minutes at room temperature, blocked and permeabilized with Fish block containing 0.2% fish skin gelatine, 1% BSA and 0.1% Triton-X (Sigma-Aldrich) for 1 hour or permeabilized for 10 minutes with Triton-X and blocked for 10 minutes with 1% BSA solution. Primary antibodies incubated for 90 minutes at room temperature and secondary antibodies mixed with DAPI (Hoechst) incubated for 1 hour at room temperature. Coverslips were mounted in a proper slide with fluoromount (Sigma-Aldrich), an aqueous based mounting medium for cover slides or with Mowiol with N-propyl-galact (Apply Chem and Sigma-Aldrich, respectively) that allows the adhesion of the coverslip on the slide. The slides were stored at 4°C in the dark. Between all the

steps, coverslips were washed 3 times with 1xPBS and before mounting the slides, coverslips were washed with distilled water.

Cells were observed with AxioImager Z1 Zeiss Microscope, using a 63x objective with the appropriate filter combination, and AxioVision software was used to process the images.

RT-qPCR

Isolation of RNA

For RNA isolation, growth medium was removed, and cells were washed with 1xPBS. Trizol (PeqLab) was added and cells were homogenized before incubating 5 minutes at room temperature. Afterwards, chloroform (for each 500µL of Tryzol, 100µL of Chloroform) was added and samples were shaken vigorously for 15 seconds. After incubating 5 minutes, samples were centrifuged for 15 minutes at 12000g and 4°C. This resulted in the phase-separation of samples where the transparent upper aqueous phase containing RNA was collected. This phase was transferred to a new tube and 250µL of isopropanol was added, which was followed by an incubation for 10 minutes on ice. The samples were centrifuged for 15 minutes at 12000g at 4°C and the resulting supernatant was removed. The pellet was washed 2x with 500µL of 75% ethanol and centrifuged for 5 minutes at 17000g, 4°C. The pellet was air-dried for 10 minutes and resuspended on 20µL of RNAse-free water (pre-heated at 55°C) and incubated for 10 minutes at 55°C. The RNA concentration was measured on nanodrop (DeNovix) and the RNA was kept at -80°C.

cDNA synthesis

cDNA synthesis was performed by mixing 2µg of extracted RNA, 280pmol of Oligo-dT primer, 166µM dNTPs, 1x Reverse transcription buffer, 20U RNAse inhibitor, 100U Reverse Transcriptase buffer and RNAse free water was added to a final volume of 30µL. The mixture was well mixed and incubated for 10 minutes at room temperature. After that, a reverse transcriptase PCR was performed by incubating for 90 minutes at 42°C, which was then followed by enzymatic inactivation for 20 minutes at 65°C (Figure 6). The cDNA obtained was kept at -20°C.

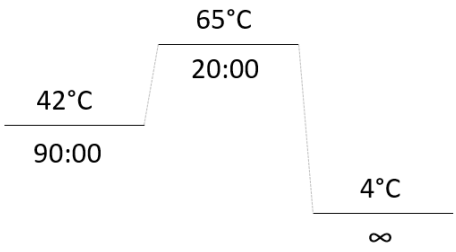

Figure 6. Reverse Transcription PCR cycle of cDNA synthesis.

Polymerase Chain Reaction and DNA electrophoresis

To check cDNA integrity, the produced cDNA was amplified by PCR and then analysed by gel electrophoresis. To do that, 2µL of cDNA was used as template, 170 nM mouse GAPDH primers, 166 µM dNTPs, 1x Reaction Buffer NZYTaq DNA Polymerase, 1.41mM MgCl2, 2.5 U NZYTaq DNA Polymerase and nuclease-free water and incubated in a thermocycler (Figure 7). The PCR products ran in a DNA electrophoresis gel in a 1% agarose gel in 1xTAE, which was stained using Midori Green DNA. To run in agarose gel, samples were mixed with 1x Orange DNA Loading Dye (ThermoFisher) and the O'GeneRuler DNA Ladder Mix (ThermoFisher) was used as marker, allowing the identification of the size. Electrophoresis was performed at 100V for 40 minutes in 1x TAE. DNA in the gel was visualized and digital images were obtain using GelDoc (BioRad).

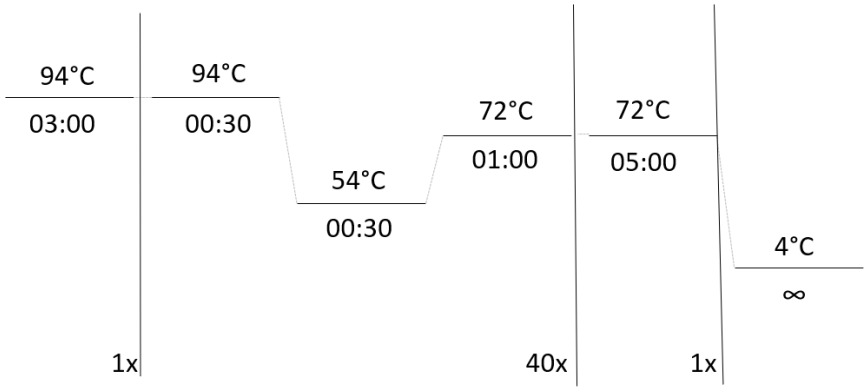

Figure 7. PCR cycle used to check cDNA integrity.

RT-qPCR reaction

For real time-quantitative polymerase chain reaction (rt-qPCR), a mastermix is prepared containing 10µL SyberGreen II Master Mix (Bimake), 1µL of 1:10 diluted primer (forward and reverse), 7µL of water and 2µL of 1:10 diluted cDNA. A 96 well plate was prepared and a programmed reaction in

which the DNA denaturation was made at 95°C for about 3 minutes, the primer annealing was made at for about 30 seconds in 40 cycles and the primer extension was made at temperature changes between 60°C and 95°C. The fluorescence was measured after the extension using the 7500 Real Time PCR System and the corresponding software from Applied Biosystems. The analysis was performed using the 2-ΔΔCT method.

The statistical analysis was performed with Graph Pad Prism® 6. Data were acquired from the quantitative analysis of IRF1 mRNA from three independent experiments and represent the means ± standard error mean (SEM). And from the quantitative analysis of ACOX1, PEX14 and Catalase mRNA from one independent experiment. To determine the significance between the experimental groups the one-way ANOVA followed by Bonferroni's multiple comparison tests were applied, where p values ≤ 0.05 were consider significant.

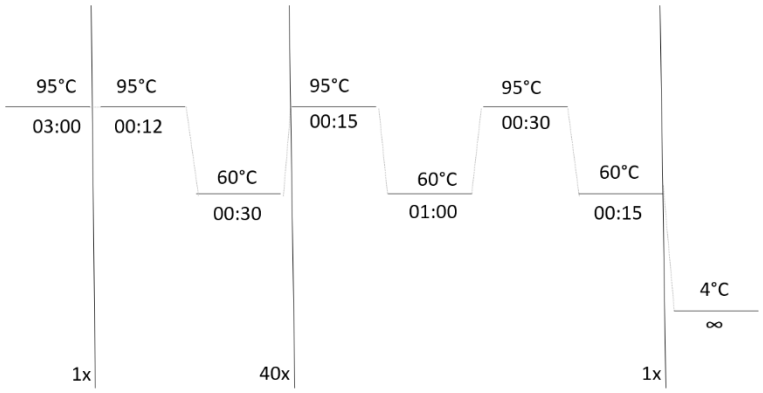

Figure 8. RT-qPCR cycling protocol.

IV. Results

IV. Results

Stimulation of RLR signalling by expression of constitutively active RIG-I does not seem to alter peroxisome metabolism

As peroxisomes are important signalling platforms for the establishment of the cellular antiviral response, we aimed unravelling whether stimulation of the RLR signalling would induce specific changes in peroxisome metabolism. To this end, we used a stimulation strategy commonly used in our group, which consists of overexpressing GFP-RIG-I-CARD, a construct that only encodes the CARD domains of RIG-I, allowing their direct interaction with the CARD domains of MAVS, hence mimicking a viral infection[60,62]. Moreover, as we previously demonstrated that HCMV vMIA strongly inhibits the peroxisomal MAVS-dependent antiviral response[60], we have also included this protein on our experimental setup, in order to investigate a possible influence on the peroxisomal metabolism.

HepG2 cells (some of which previously transfected with vMIA-myc 24hrs earlier) were transfected with GFP-RIG-I-CARD for 6hrs. Each construct was transfected alone as a control. HepG2 cells were choose for these studies for being widely used in studies of intracellular protein trafficking. The successful transfections were confirmed by immunofluorescence followed by microscopy analysis (Figure 9).

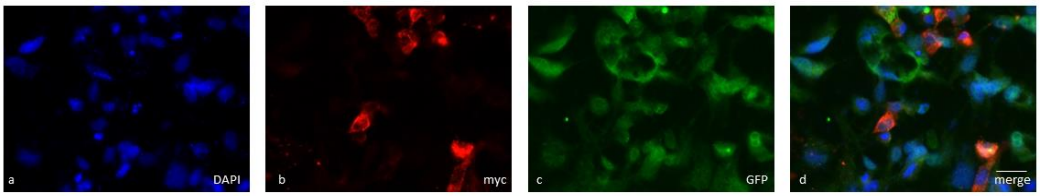

Figure 9. HepG2 cells transfected with GFP-RIG-I-CARD and vMIA-myc. (a) DAPI, (b) myc, (c) GFP, (d) merge of a-c. Scale bar corresponds to 10µm.

Antibodies against the following proteins were used: PMP70, a branched-chain fatty acid transporter; PEX14, a component of the peroxisomal import machinery also known to be involved in peroxisomes movement; ACOX1, which is a peroxisomal acyl-coenzyme A oxidase 1 involved in the VLCFA β-oxidation; and Catalase, responsible for ROS degradation at peroxisomes. The results presented in Figure 10A do not show any visible differences between un-stimulated and stimulated (in the presence or absence of vMIA) cells. To confirm these results, protein quantity was accessed

by band intensity quantification. Protein bands intensity were compared and normalized against the bands intensity of the housekeeping gene, α/β-tubulin. This analysis confirmed that no significant differences were observed (Figure 10B).

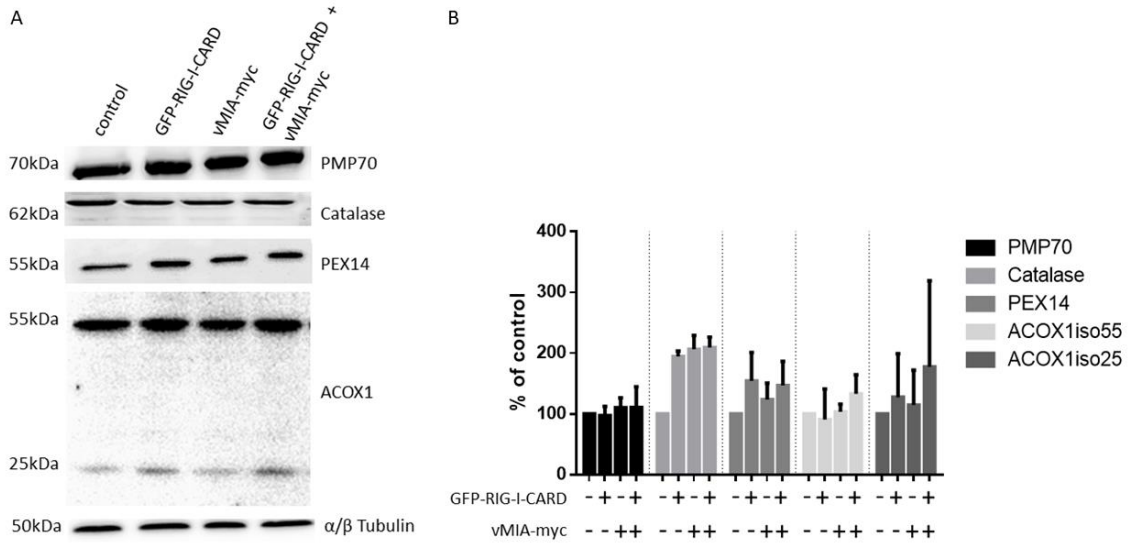

Figure 10. HepG2 cells were stimulated by GFP-RIG-I-CARD in the presence or absence of vMIA-myc and analysed (A) by immunoblotting. (B) Quantification of band intensity. Tubulin was used as normalizer gene. Data represents the means ± SEM of three independent experiments. Statistical analysis was performed using one-way ANOVA followed by Bonferroni's multiple comparison. Quantification made with Quantity One.

We have also decided to analyse the mRNA expression of PEX14, ACOX1 and Catalase through RT-qPCR in the MEFs MAVS-PEX cells[60] that contains MAVS solely at peroxisomes. To this end, we stimulated these cells (some of them previously transfected with vMIA-myc for 24hrs) by transfecting GFP-RIG-I-CARD. After 6hrs, cells were collected, and RT-qPCR was performed to measure the mRNA expression of ACOX1, PEX14 and Catalase. Figure 11 shows that there is no significant alteration on the mRNA production of the selected peroxisomal genes.

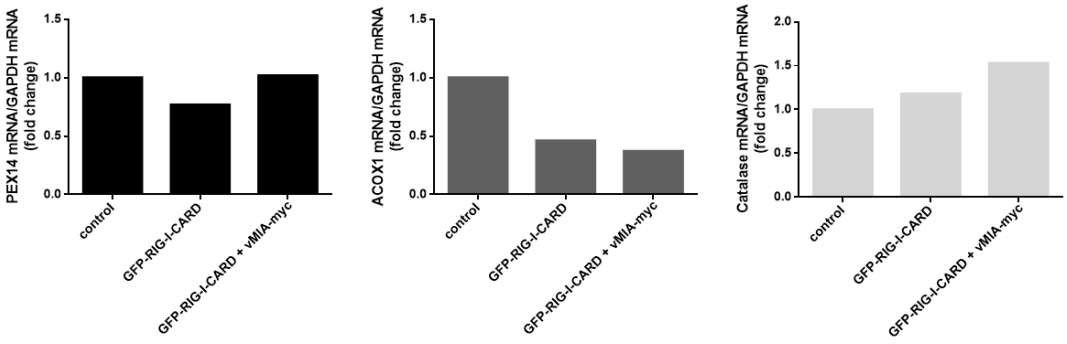

Figure 11. mRNA expression of PEX14, Catalase and ACOX1 does not alter with the activation of the peroxisomal MAVS-dependent antiviral response or by the presence of vMIA in MEFs MAVS-PEX cells. GAPDH was used as normalizer gene. Data represents one independent experiment.

Sendai virus infection does not seem to alter peroxisome metabolism

Complementing the previous results, we wondered if the absence of alterations in peroxisome metabolism, after stimulation of the RLR antiviral signalling, could be associated to the type of stimulus used to induce the cellular antiviral response. Thus, we decided to infect the cells with Sendai virus (SeV) as a stimulus. SeV is a RNA virus from the *Paramyxoviridae* family, closely related to the parainfluenza virus-1 and parainfluenza virus-3[63], with a broad cellular tropism, infecting almost all type of cells and tissues[42]. To this end HEK 293T cells were infected with SeV, in the presence or absence of vMIA. Eight hours post infection immunoblotting analysis was performed and antibodies against Catalase, ACOX1 and PEX14 were used. As it is possible to observe in Figure 12A, no visible differences are detected. To confirm these results, protein quantity was accessed by band intensity quantification, as previous indicated. This analysis confirmed that no significant differences exist (Figure 12B).

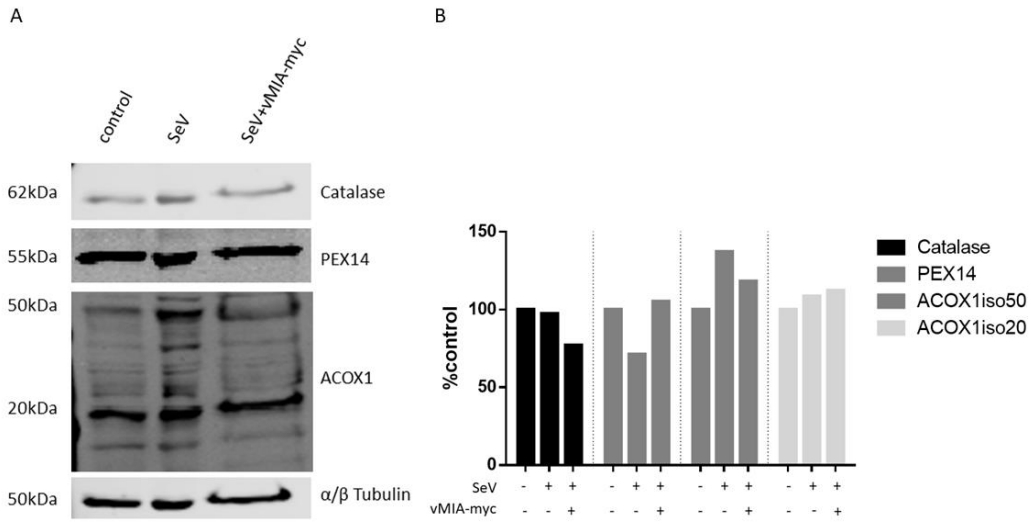

Figure 12. HEK293T cells were infected with Sendai Virus in the presence or absence of vMIA-myc and analysed (A) by immunoblotting. (B) Quantification of band intensity. Tubulin was used as normalizer gene. Data represents one independent experiment. Quantification made with Quantity One.

FTIR analysis of cellular metabolism upon RLR signalling activation

In parallel, we performed metabolic analysis using the Fourier Transformed InfraRed (FTIR) Spectroscopy. FTIR is a spectroscopy technique that is gaining visibility in biomedical research and takes advantage of the absorbance of infrared radiation by biological samples. This technique is relatively simple, cheap, fast to analyse, reproducible and it is non-destructive to samples. Moreover, it can be done with small amounts of sample, with no need of too much preparation.

To perform these analyses, we stimulated HepG2 cells with GFP-RIG-I-CARD (R*) for 6hrs, in the presence or absence of vMIA-myc (R+V*, 24hrs before RIG-I-CARD). As controls, we used non-stimulated cells (C*), cells transfected only with an empty vector (EV*) and cells only transfected with vMIA (V*, *further on the results will be referred by these abbreviations).

The analysis of the results was made with the Unscrambler® (CAMO) and results were excluded when samples presented extensive noise. The spectra obtained were divided between 4000-600cm^{-1} into regions of interest, since the region between 3000-2700cm^{-1} is a lipid dominated region (except for some contributions from proteins) and the region between 1800-900cm^{-1} is referred as a fingerprint region, which allows the identification of proteins, protein structures and nucleic acids. Specifically bands at 1653cm^{-1} (Amide I) and 1544cm^{-1} (Amide II) are characteristic of bond vibrations from proteins[64] (Figure 13).

Principal Component Analysis (PCA) of normalized 2nd derivative spectra was used to infer the differences between the conditions and to measure the variability between samples[65]. The assignments of peaks identified in this study were made based on previous FTIR studies on whole cells, organelles, and macromolecules[66].

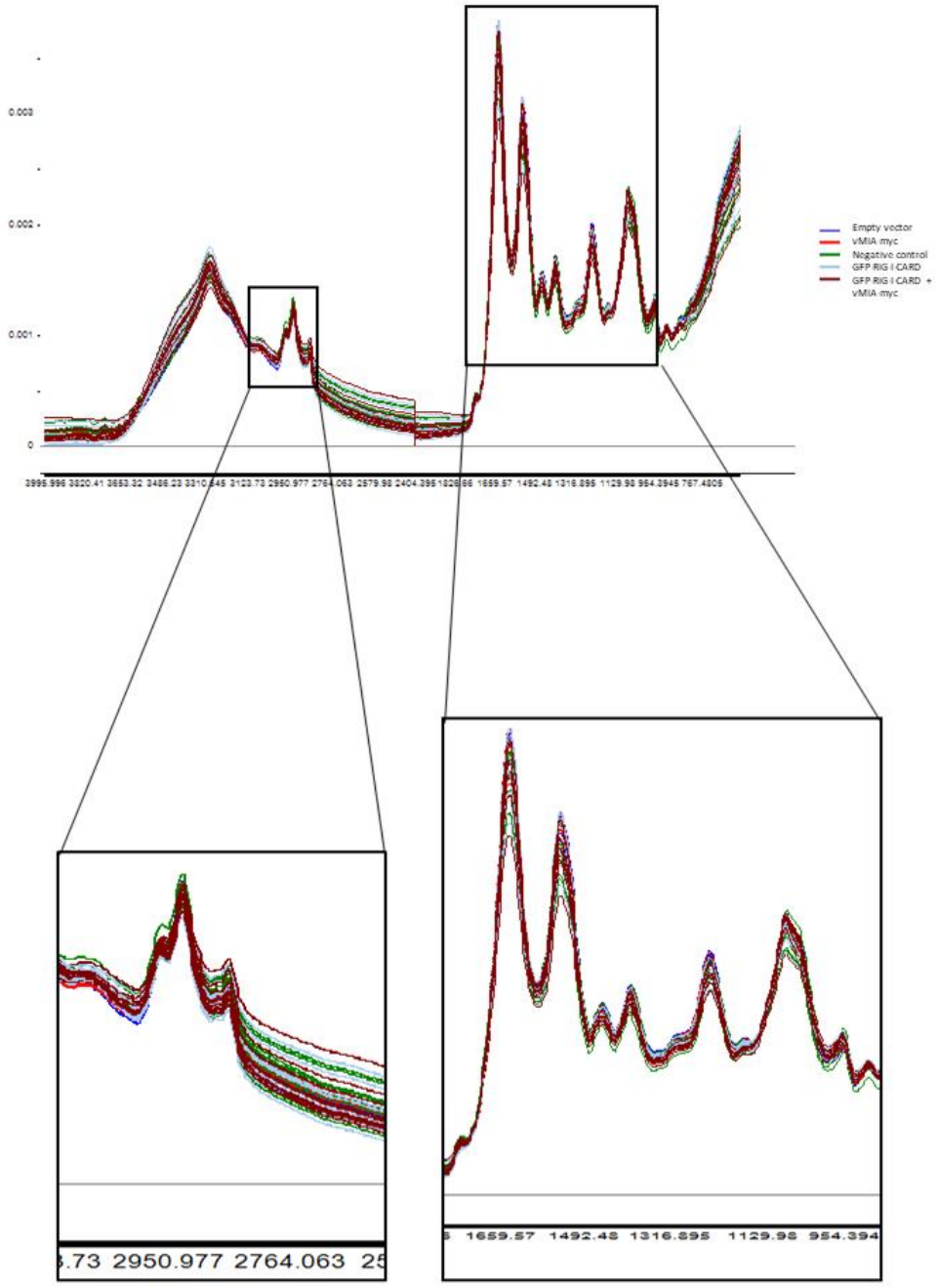

Figure 13. FTIR spectra of normalized spectra in the region 4000-600cm^{-1}, from HepG2 cells transfected with GFP-RIG-I-CARD for 6 hrs in the presence or absence of vMIA-myc. Non-stimulated cells, cells transfected with an empty vector or only with vMIA were used as controls. Amplification of the regions between 3000 and 2800cm^{-1} (right) and 1800 and 900cm^{-1} (left). x-axis: wavenumber (cm^{-1}); y-axis: arbitrary units (AU). Absorbance (arbitrary units (AU)).

Regarding the lipid region and despite the high dispersion of samples, PC1 was used to separate this region. This component spans the variance between the samples *C*, *R* and *R+V* from the samples *V* and *EV*, explaining 83% of the variance (Figure 14A). When analysing the loading plot, which translates the weight of each PCA analysis on a total analysis, it is observed that three main wavenumbers contributed to the variance that exists along PC1: 2851cm^{-1}, 2922cm^{-1} and 2945cm^{-1} (Figure 14B). These bands correspond to stretching vibrations of CH_2 and CH_3 of phospholipids, cholesterol and creatinine, as well as CH stretching vibrations of lipids and methyl groups. Precisely, these bands correspond to symmetric CH_2 stretching (2851cm^{-1}), asymmetric stretching vibration of CH_2 of acyl chains (lipids) (2922cm^{-1}) and stretching C-H (2946/2948cm^{-1})[67]. The position where is observed a CH_2 stretching absorption on protein structure can provide important information regarding the packing characteristics of the acyl chain of a organelle membrane, which in turn may be related to the degree of fluidity of the lipid membrane, which does not show a considerable difference on our samples[68].

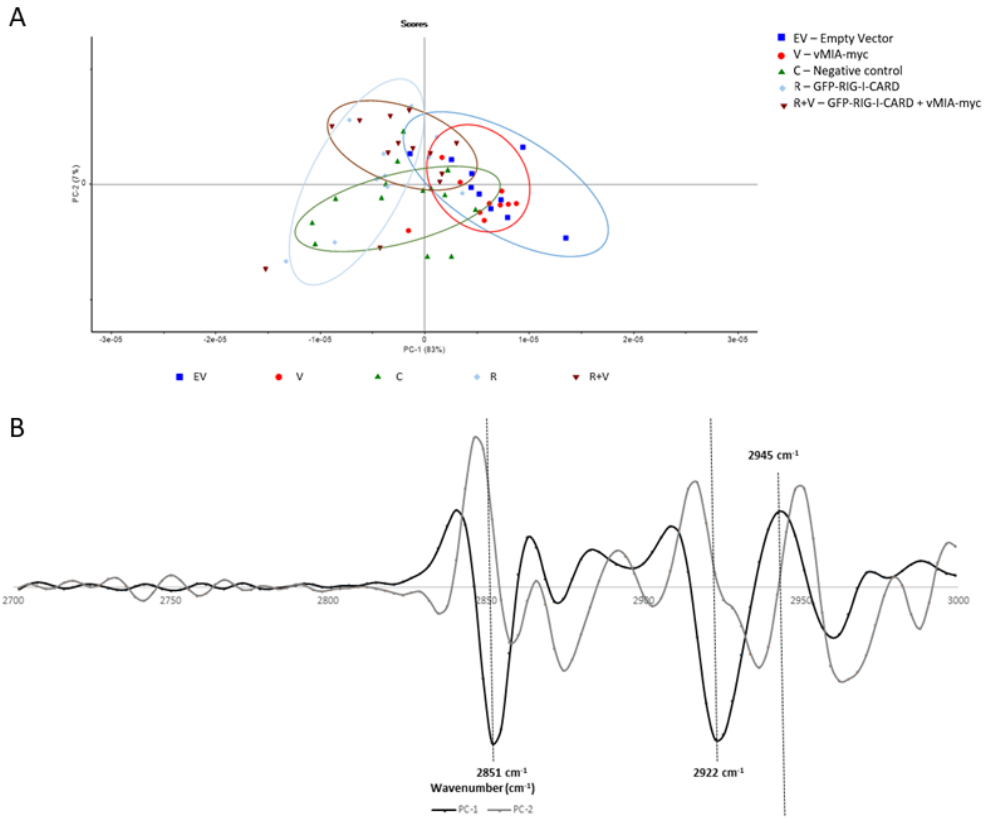

Figure 14. PCA score (A) and loadings (B) plots, of normalized second derivative spectra at the region 3000-2700cm^{-1} from HepG2 cells transfected with GFP-RIG-I-CARD for 6 hrs in the presence or absence of vMIA-myc. Non-stimulated cells, cells transfected with an empty vector or only with vMIA were used as controls.

Then, we analysed the region between 1600 and 1700cm^{-1}, as it corresponds to the region that allows us to deduce the secondary structure of the proteins in each sample. Although some dispersion is observed it is possible to detect some tendency for the separation according to PC1 component. The PC1 spans the variance between mainly the samples *R* and *EV* from the samples *C*, *R+V* and V, explaining 62% of the variation (Figure 15A). The loading plot revealed five of the main variables contributing to the variance present along PC2, which are the absorption bands at 1651cm^{-1}, 1682cm^{-1}, 1699cm^{-1}, 1659cm^{-1} and 1690cm^{-1} (Figure 15B). These bands correspond mainly to Amide I region, where at 1699cm^{-1} it is present a vibration between antiparallel β-sheets that is described profile for oligomers. Also, the 1690cm^{-1} region corresponds to nucleic acids due to the base carbonyl stretching and the ring breathing mode[67].

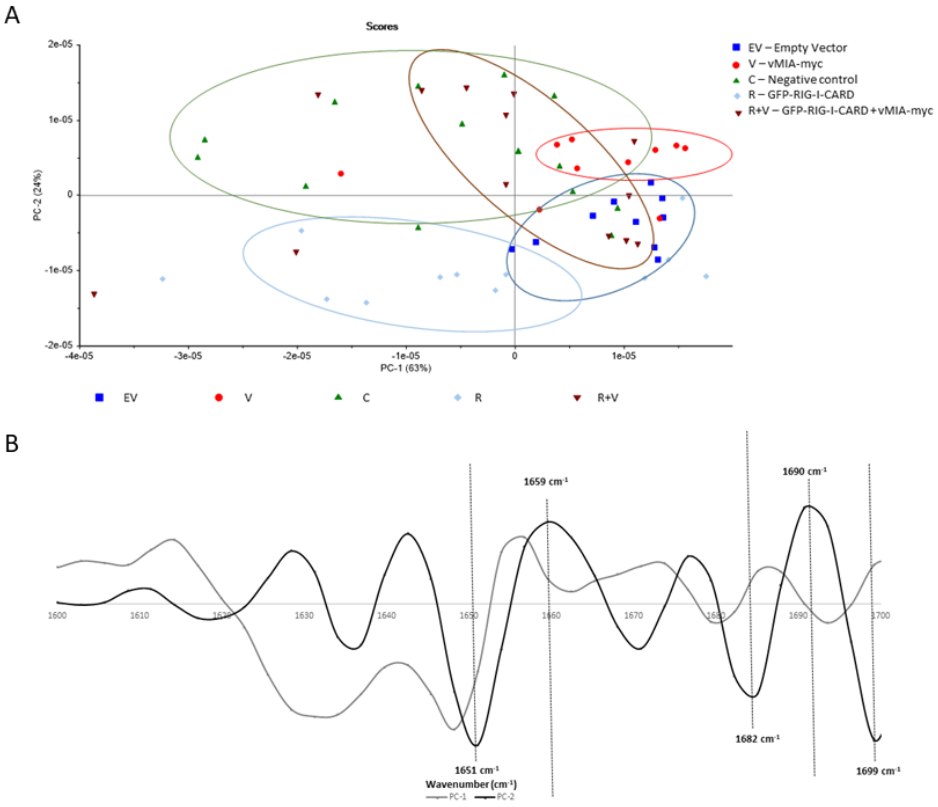

Figure 15. PCA score (A) and loadings (B) plots from the normalized second derivative spectra at the region 1700-1600cm^{-1}, from HepG2 cells transfected with GFP-RIG-I-CARD for 6hrs in the presence or absence of vMIA-myc. Non-stimulated cells, cells transfected with an empty vector or only with vMIA were used as controls.

The protein region between 1600-1500cm^{-1} was also analysed in detail. It is possible to observe a tendency for division according to PC2 analysis. This component spans the variance between the samples *C*, *R+V* and *V* from the samples *R* and *EV*, explaining 26% of the observed variance (Figure 16A). When studying the loading plot, it is revealed that three of the main variables contributing to variance explanation along PC2 are the absorption bands at 1540cm^{-1}, 1557cm^{-1} and 1549cm^{-1} (Figure 16B). These bands correspond to the presence of protein amide II absorption, predominantly β-sheet of amide II[67]. However, this region is not sensible to conformational changes as reported for amide I, so analysis is only made considering only the amide I region[69].

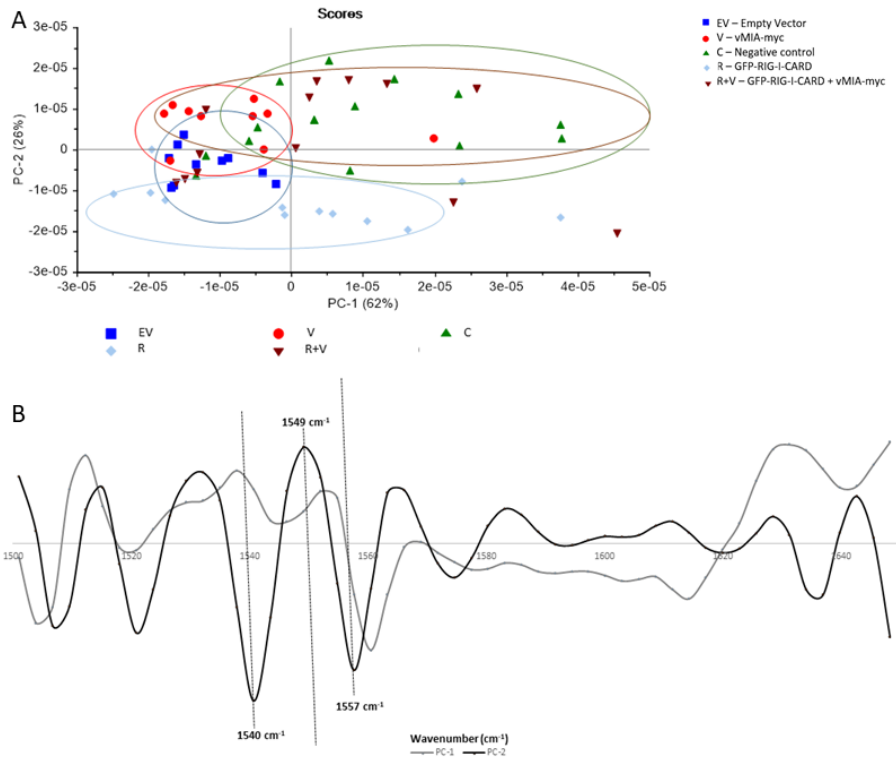

Figure 16. PCA score (A) and loadings (B) plots from the normalized second derivative spectra at the region 1600-1500cm^{-1}, from HepG2 cells transfected with GFP-RIG-I-CARD for 6hrs in the presence or absence of vMIA-myc. Non-stimulated cells, cells transfected with an empty vector or only with vMIA were used as controls.

Finally, we analysed the region between 1350-900cm^{-1} that includes the region of nucleic acids, phospholipids and fatty acids. After PCA analysis, it is possible to observe a separation with PC1, which spans the variance between the samples *R*, *C* and *R+V* from the samples *EV* and *V*, explaining 42% of the variance (Figure 17A). The loadings plot revealed three main variables that contribute to the variance along PC1, which correspond to the absorption bands at 982cm^{-1}, 1070cm^{-1} and at 1084cm^{-1} (Figure 17B). These bands correspond to nucleic acids (1070cm^{-1}) and to PO^{-}_{2} stretching vibrations, characteristic of DNA[67]. Since DNA transfections were performed, it was expected to observe more stretching absorption from DNA and RNA[68].

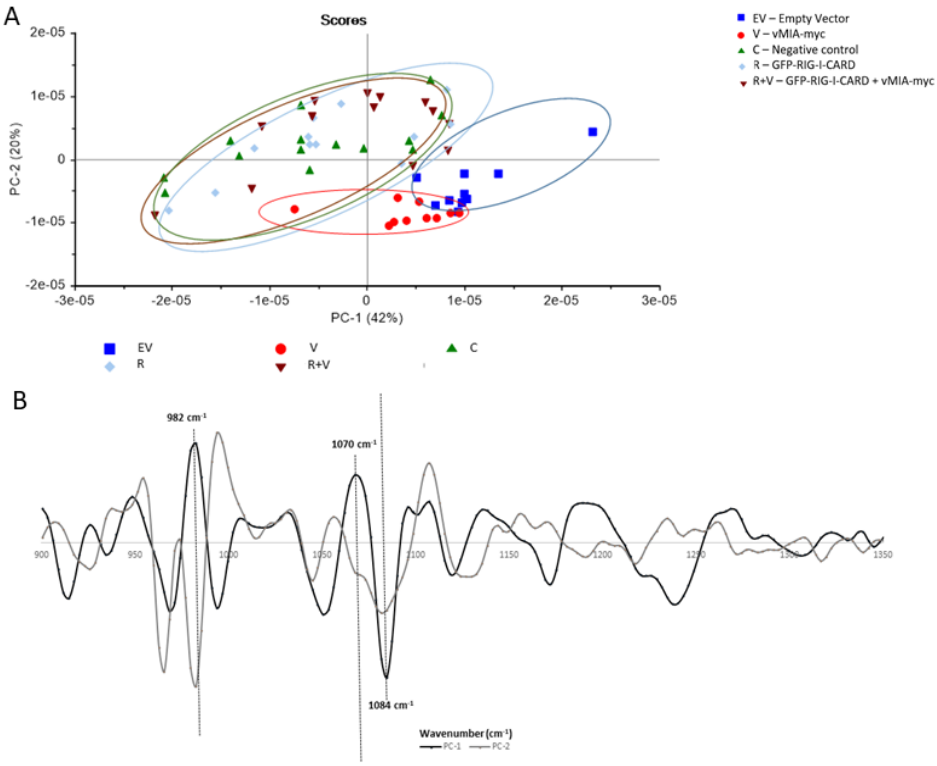

Figure 17. PCA score (A) and loadings (B) plots of the normalized second derivative spectra at the region 1350-900cm^{-1}, from HepG2 cells transfected with GFP-RIG-I-CARD for 6hrs in the presence or absence of vMIA-myc. Non-stimulated cells, cells transfected with and empty vector or only with vMIA were used as controls.

ACBD5 is required for an effective RLR antiviral response

ACBD5 is the tether protein that stabilizes the interaction between ER and peroxisomes, by interacting with VAPB, an ER tail anchored ER protein that functions as an adaptor in inter-organellar lipid exchange and membrane tethering[26]. Their interaction allows the exchange of lipids between the two organelles substantiating their importance in peroxisome biogenesis, as well as synthesis of plasmogens, ether phospholipids and cholesterol precursors[26,28].

ER and peroxisomes are both involved in the cellular defence: ER harbours STING, the adaptor protein in viral DNA sensing, while peroxisomes are signalling platforms for viral RNA sensing due to the presence of MAVS, at this organelle. In order to test the importance of ACBD5 (and further infer on a possible role of the peroxisome-ER interactions) for the cellular antiviral defence. MEFs with a knock-out on the ACBD5 gene (MEFs ACBD5 KO cells) were stimulated with GFP-RIG-I-CARD for 6 hrs. As control, MEFs wild type (MEFs WT) cells were used and similarly processed. RT-qPCR analysis of the production of the ISG IRF1 was used to determine the antiviral response.

The results in Figure 18 demonstrate that stimulated MEFs ACBD5-KO cells were incapable of expressing the same levels of IRF1 as MEFs WT cells, suggesting that ACBD5 may be important for the cellular antiviral immune defence.

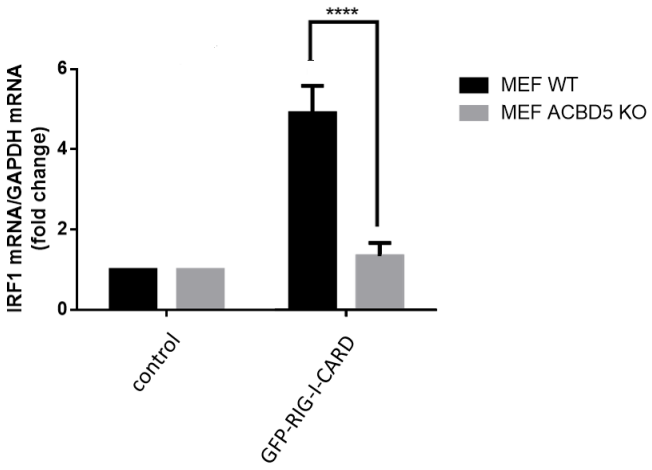

*Figure 18. Analysis of IRF1 mRNA production by RT-qPCR of MEFs WT and MEFs ACBD5 KO stimulated with GFP-RIG-I-CARD. GAPDH was used as a normalizer gene. Data represents the means ± SEM of 3 independent experiments. Statistical analysis was performed using one-way ANOVA followed by Bonferroni's multiple comparison. Error bars represent SEM ****p≤0.0001 compared with control.*

V. Discussion

V. Discussion

Peroxisomes are important organelles for cellular survival and homeostasis maintenance. They are recognized for their functions on the metabolism of lipids and ROS, and their role on the antiviral innate immunity.

Recent studies have already pinpointed the importance of peroxisome metabolism on specific viral infections. In fact, a study demonstrated the importance of the peroxisomal lipid metabolism in influenza virus production, since viral proliferation is dependent of three major metabolic pathways: elevated ether lipids, sphingolipids biosynthesis for virus morphogenesis and decreased peroxisomal β-oxidation for intracellular life cycle stages[70]. A recent study referred that enveloped virus like herpes simplex virus type I (HSV-I) and HCMV induces plasmogens production by peroxisomes, which are essential for their assembly. Also, other proteomic study have shown that ROS metabolism and fatty acid oxidation are increased during enveloped viruses infection[71]. Although the mechanisms associated are yet to be elucidated, latent herpesvirus infection also manipulates peroxisomal lipid signalling, through ACOX1 and ABCD3 (PMP70) which are required for survival in a long term infection[72].

With the aim of unravelling the role of peroxisomes metabolism for the establishment of the antiviral response, we have analysed different metabolical functions of peroxisomes upon activation of the RLR antiviral signalling. Our results show that activation of RLR signalling, using a constitutively active version of RIG-I, which mimics viral infection, does not alter the protein levels of PMP70, PEX14, ACOX1 or catalase. These proteins are involved in different metabolic functions of peroxisomes: PMP70 is responsible for the import of VLCFA into peroxisomes, PEX14 belongs to the peroxisomal import machinery, essential for peroxisome biogenesis, ACOX1 is a peroxisomal oxidase in VLCFA β-oxidation and catalase degrades the ROS produced by peroxisomes. Moreover, we have also quantified the mRNA production and, as observed on protein level, no alterations were observed. We have also analysed peroxisomal proteins levels upon SeV infection, but, as previously, no alterations were observed. This could be explained by the time point upon infection of stimulation with GFP-RIG-I-CARD on which we analysed peroxisomal proteins. To confirm these results, peroxisomal proteins should be analysed at different time points, and other techniques to analyse peroxisome functions should be applied.

We have also performed FTIR analysis, upon stimulation of RLR signalling. This is a very useful technique in the biomedical field that allows a rapid and reproducible assessment of the metabolic

cell profile. Besides, it is relatively narrow since it permits the rapid collection of spectra, obtained from small well-defined spatial regions, of around 7x7μm^2, that can be scanned to provide a biochemical map, which it is easy to resolve, sensitive to molecular structure, conformation and to the environment[73]. One of the main disadvantages of FTIR is that this technique does not allow the identification of specific compounds, and to overcome this, complementary techniques are necessary to confirm FTIR results[67].

Our FTIR results show that the stimulation of the RLR signalling, using GFP-RIG-I-CARD to mimic infection, induces an increase of β-sheets vibration, while stimulation in the presence of vMIA-myc presents the same signal as the negative control. It has been described that β-sheet vibration is a common signal for oligomerized proteins[74]. This signal is common in samples that present proteins oligomers and may be consistent with the induction of MAVS oligomerization when the RLR signalling is activated. Moreover, it has been shown that vMIA inhibits MAVS activation[58,60], explaining the absence of β-sheets vibration on the samples that were stimulated with RIG-I-CARD in the presence of vMIA. Regarding the bands that identify differences on lipids or nucleic acids, no big differences were observed. Once again, we propose that these studies should be repeated at different time points after stimulation.

ACBD5 has been described as a protein localized at peroxisomal membranes and indispensable for the establishment of peroxisome-ER interaction, coordinating lipid transfer between these two organelles[26,28]. Both ER and peroxisomes have been described as signalling platforms in cellular antiviral defence, each one harbouring adaptor proteins essential for the signalling in response to viral DNA and RNA, respectively. Interestingly, the stimulation of the RLR signalling in cells that lack ACBD5 did not induce the expression of ISGs, as it was observed in wild type cells. These results suggest that ACBD5 is essential for the RLR antiviral signalling, possibly by stabilizing ER-peroxisomes interaction or due to its role on the import of lipids to peroxisomes. Moreover, it enforces the importance of inter-organellar communication in antiviral immunity, as it was observed for mitochondria-peroxisomes communication as signalling platforms in the RLR antiviral signalling. Further studies should address which of the functions of ACBD5 are essential for the RLR signalling pathway. Moreover, it would be interesting to study if the peroxisomes-ER communication affects the STING-dependent antiviral response.

VI. Conclusion

VI. Conclusion

Peroxisomes are important organelles for human health and essential for many cellular metabolic pathways, as well as for the RLR-mediated antiviral innate immune response. Moreover, peroxisomes establish contacts with several organelles, allowing their cooperation in the maintenance of cellular homeostasis.

This work makes us conclude two main points:

1. Activation of RLR antiviral signalling does not seem to induce any differences on peroxisomal metabolic functions;
2. ACBD5 seems to be essential for the peroxisome-mediated RLR antiviral response.

The results obtained with this work allow a new perspective on the role of peroxisomes as signalling platforms on RLR antiviral signalling and further studies are proposed in order to better clarify their role on cellular antiviral immunity.

VII. References

VII. References

1. Duve, C. & Baudhuin, P. Peroxisomes (Microbodies and Related Particles). *Am. Physiol. Soc.* **46,** 323–357 (1966).

2. Schrader, M. & Fahimi, H. D. The peroxisome: Still a mysterious organelle. *Histochem. Cell Biol.* **129,** 421–440 (2008).

3. Wanders, R. J. A. Metabolic functions of peroxisomes in health and disease. *Biochimie* **98,** 36–44 (2014).

4. Islinger, M., Grille, S., Fahimi, H. D. & Schrader, M. The peroxisome: An update on mysteries 2.0. *Histochem. Cell Biol.* **137,** 547–574 (2012).

5. Tabak, H. F., Braakman, I. & Zand, A. van der. Peroxisome Formation and Maintenance Are Dependent on the Endoplasmic Reticulum. *Annu. Rev. Biochem.* **82,** 723–744 (2013).

6. Agrawal, G. & Subramani, S. De novo peroxisome biogenesis: evolving concepts and conundrums. *Biochim Biophys Acta* **1863,** 892–901 (2016).

7. Sugiura, A., Mattie, S., Prudent, J. & Mcbride, H. M. Newly born peroxisomes are a hybrid of mitochondrial and ER-derived pre-peroxisomes. *Nature* **542,** 251–254 (2017).

8. Kim, P. Peroxisome Biogenesis: A Union between Two Organelles. *Curr. Biol.* **27,** R271–R274 (2017).

9. Dias, A. F. *et al.* The peroxisomal matrix protein translocon is a large cavity- forming protein assembly into which PEX5 protein enters to release its cargo. *Am. Soc. Biochem. Mol. Biol.* **292,** 15287–15300 (2017).

10. Otera, H. *et al.* Peroxisome Targeting Signal Type 1 (PTS1) Receptor Is Involved in Import of Both PTS1 and PTS2: Studies with PEX5-Defective CHO Cell Mutants. *Mol. Cell. Biol.* **18,** 388–399 (1998).

11. Fujiki, Y. Approaches to studies on peroxisome biogenesis and human peroxisome-deficient disorders. *Ann. N. Y. Acad. Sci.* **804,** 491–501 (1996).

12. Yoshida, Y., Niwa, H., Honsho, M., Itoyama, A. & Fujiki, Y. Pex11p mediates peroxisomal

proliferation by promoting deformation of the lipid membrane. (2015). doi:10.1242/bio.20149654

13. Katarzyna, Z., Suresh, S. & Diego, S. Autophagic degradation of peroxisomes in mammals. *Biochem Soc Trans* **44,** 431–440 (2016).

14. Eberhart, T. & Kovacs, W. J. Pexophagy in yeast and mammals: an update on mysteries. *Histochem. Cell Biol.* **150,** 473–488 (2018).

15. Cuervo, A. M. & Wong, E. Chaperone-mediated autophagy: roles in disease and aging. *Cell Res.* **24,** 92–104 (2014).

16. Wanders, R. J. A. & Waterham, H. R. Biochemistry of Mammalian Peroxisomes Revisited. *Annu. Rev. Biochem.* **75,** 295–332 (2006).

17. Hajra, A. K. & Das, A. K. Lipid Biosynthesis in Peroxisomes. *Annals of the New York Academy of Sciences.* 804, 129-141 (1996). doi:10.1111/j.1365-3040.2007.01761.x

18. Hiltunen, J. K., Karki, T., Hassinen, I. E. & Osmundsen, H. Beta-oxidation of polyunsaturated fatty acids by mt liver peroxisomes. A role for 2,4-dienoyl-coenzyme a reductase in peroxisomal beta-oxidation. *J. Biol. Chem.* **261,** 16484–16493 (1986).

19. Poirier, Y., Antonenkov, V. D., Glumoff, T. & Hiltunen, J. K. Peroxisomal β-oxidation-A metabolic pathway with multiple functions. *Biochim. Biophys. Acta - Mol. Cell Res.* **1763,** 1413–1426 (2006).

20. Camões, F., Islinger, M., Guimarães, S. C., Kilaru, S., Schuster, M., Godinho, L. F., Steinberg G., Schrader M. New insights into the peroxisomal protein inventory : Acyl-CoA oxidases and -dehydrogenases are an ancient feature of peroxisomes. *Biochim. Biophys. Acta* **1853,** 111–125 (2015).

21. Schrader, M., Godinho, L. F., Costello, J. L. & Islinger, M. The different facets of organelle interplay—an overview of organelle interactions. *Front. Cell Dev. Biol.* **3,** 1–22 (2015).

22. Chu, B. *et al.* Cholesterol Transport through Lysosome- Peroxisome Membrane Contacts Cholesterol Transport through Lysosome-Peroxisome Membrane Contacts. *Cell* **161,** 291–306 (2015).

23. Novikoff, A. & Shin, W. Y. The endoplasmic reticulum in the Golgi zone and its relation to microbodies, Golgi apparatus and autophagic vacuoles in rat liver cells. *J. Microsc.* **3,** 187–206 (1964).

24. Costello, J. L., Castro, I. G., Schrader, T. A., Islinger, M. & Schrader, M. Peroxisomal ACBD4 interacts with VAPB and promotes ER-peroxisome associations. *Cell Cycle* **16,** 1039–1045 (2017).

25. Zand, A. van der, Braakman, I. & Tabak, H. F. Peroxisomal Membrane Proteins Insert into the Endoplasmic Reticulum. *Mol. Biol. Cell* **21,** 2057–2065 (2010).

26. Costello, J. L. *et al.* ACBD5 and VAPB mediate membrane associations between peroxisomes and the ER. *J. Cell Biol.* **216,** 331–342 (2017).

27. Neess, D., Bek, S., Engelsby, H., Gallego, S. F. & Færgeman, N. J. Progress in Lipid Research Long-chain acyl-CoA esters in metabolism and signaling : Role of acyl-CoA binding proteins. *Prog. Lipid Res.* **59,** 1–25 (2015).

28. Hua, R. *et al.* VAPs and ACBD5 tether peroxisomes to the ER for peroxisome maintenance and lipid homeostasis. *J. Cell Biol.* **216,** 367–377 (2017).

29. Ferdinandusse, S. *et al.* ACBD5 deficiency causes a defect in peroxisomal very long-chain fatty acid metabolism. *J. Med. Genet.* **54,** 330–337 (2017).

30. Fransen, M., Nordgren, M. & Wang, B. *Peroxisomes and their Key Role in Cellular Signaling and Metabolism*. (Springer Berlin Heidelberg, 2013).

31. Dixit, E. *et al.* Peroxisomes are signaling platforms for antiviral innate immunity. *Cell* **141,** 668–681 (2010).

32. Bongarzone, E. R., Givogri, M. I., Vivo, D. C. De & Dimauro, S. Inborn Metabolic Defects of Lysosomes, Peroxisomes, Carbohydrates, Fatty Acids and Mitochondria. in *Diseases of Carbohydrate and fatty acids* 755–779 (Elsevier Inc., 2012). doi:10.1016/B978-0-12-374947-5.00067-5

33. Wanders, R. J. A. & Waterham, H. R. Peroxisomal disorders: The single peroxisomal enzyme deficiencies. *Biochim. Biophys. Acta - Mol. Cell Res.* **1763,** 1707–1720 (2006).

34. Shimozawa, N. Molecular and clinical aspects of peroxisomal diseases. *J. Inherit. Metab. Dis.* **30,** 193–197 (2007).

35. Marques, M., Ferreira, A. R. & Ribeiro, D. The Interplay between Human Cytomegalovirus and Pathogen Recognition Receptor Signaling. *Viruses* (2018). doi:10.3390/v10100514

36. Hug, H., Mohajeri, M. H. & La Fata, G. Toll-like receptors: Regulators of the immune response in the human gut. *Nutrients* **10,** 11–13 (2018).

37. Saito, T. *et al.* Regulation of innate antiviral defenses through a shared repressor domain in RIG-I and LGP2. *Proc. Natl. Acad. Sci.* **104,** 582–587 (2007).

38. Meylan, E. *et al.* Cardif is an adaptor protein in the RIG-I antiviral pathway and is targeted by hepatitis C virus. *Nature* **437,** 1167–1172 (2005).

39. Hou, F. *et al.* MAVS Forms Functional Prion-Like Aggregates To Activate and Propagate Antiviral Innate Immune Response. *Cell* **146,** 448–461 (2011).

40. Vallabhapurapu, S. & Karin, M. Regulation and Function of NF-κB Transcription Factors in the Immune System. *Annu. Rev. Immunol.* **27,** 693–733 (2009).

41. Paz, S. *et al.* A functional C-terminal TRAF3-binding site in MAVS participates in positive and negative regulation of the IFN antiviral response. *Nat. Publ. Gr.* **21,** 895–910 (2011).

42. Seth, R. B., Sun, L., Ea, C. K. & Chen, Z. J. Identification and characterization of MAVS, a mitochondrial antiviral signaling protein that activates NF-κB and IRF3. *Cell* **122,** 669–682 (2005).

43. Liu, Y., Olagnier, D. & Lin, R. Host and viral modulation of RIG-I-mediated antiviral immunity. *Front. Immunol.* **7,** 1–12 (2017).

44. Odendall, C. & Kagan, J. C. Peroxisomes and their Key Role in Cellular Signaling and Metabolism. *Subcell Biochem.* **69,** 67–75 (2013).

45. Sun, L., Wu, J., Du, F., Chen, X. & Chen, Z. J. Cyclic GMP-AMP Synthase is a Cytosolic DNA Sensor that Activates the Type-I Interferon Pathway. *Science (80-.).* **339,** (2013).

46. Bowie, A. *et al.* A46R and A52R from vaccinia virus are antagonists of host IL-1 and toll-like

receptor signaling. *Proc. Natl. Acad. Sci. U. S. A.* **97,** 10162–7 (2000).

47. Chow, J., Franz, K. M. & Kagan, J. C. PRRs are watching you: Localization of innate sensing and signaling regulators. *Virology* 104–109 (2015). doi:10.1038/nrg3575.Systems

48. Nightingale, K., Lin, K. M., Ravenhill, B. J., Stanton R. J., Tomasec P., Weekes M.P. High-Definition Analysis of Host Protein Stability during Human Cytomegalovirus Infection Reveals Antiviral Factors and Viral Evasion Mechanisms. *Cell Host Microbe* **24,** 447–460.e11 (2018).

49. Britt, W. J. & Prichard, M. N. New therapies for human cytomegalovirus infections. *Antiviral Res.* (2018). doi:10.1016/j.antiviral.2018.09.003

50. Stern-Ginossar, N., Weisburd, B., Michalski, A., Le,V. T. K., Hein, M. Y., Huang, S. H., Ma, M., Shen, B., Qian S. B., Hengel, H., Mann, M., Ingolia, N. T., Weissman J. S. Decoding human cytomegalovirus. *Science.* **338,** 1088–1093 (2012).

51. Bresnahan, W. A., Shenk, T., Bresnahan, W. A. & Shenk, T. A Subset of Viral Transcripts Packaged within Human Cytomegalovirus Particles Published by : American Association for the Advancement of Science Stable URL : http://www.jstor.org/stable/3075592 A Subset of Viral Transcripts Packaged Within Human Cytomegal. *Sci. Am. Assoc. Adv. Sci.* **288,** 2373–2376 (2000).

52. Murphy, E., Vanicek, J., Robins, H., Shenk, T. & Levine, A. J. Suppression of immediate-early viral gene expression by herpesvirus-coded microRNAs: Implications for latency. *Proc. Natl. Acad. Sci.* **105,** 5453–5458 (2008).

53. Scherer, M., Otto, V., Stump, J. D., Klingl S., Mueller, R., Reuter, N., Muller, Y. A., Sticht, H., Stamminger, T. Characterization of Recombinant Human Cytomegaloviruses Encoding IE1 Mutants L174P and 1-382 Reveals that Viral Targeting of PML Bodies Perturbs both Intrinsic and Innate Immune Responses. *J. Virol.* **90,** 1190–1205 (2016).

54. Arvin, A. *et al. Human Herpesviruses. Biology, Therapy, and Immunoprophylaxis.* (2007).

55. Fu, Y., Su, S., Gao, Y., Wang, P., Huang, Z., Hu, M., Luo, W. Li, S., Luo M. Human Cytomegalovirus Tegument Protein UL82 Article Human Cytomegalovirus Tegument Protein UL82 Inhibits STING-Mediated Signaling to Evade Antiviral Immunity. *Cell Host Microbe* **21,**

231–243 (2017).

56. Kim, J.-E., Kim, Y., Stinski, M. F., Ahn, J. & Song, Y. Human Cytomegalovirus IE2 86 kDa Protein Induces STING Degradation and Inhibits cGAMP-Mediated IFN-beta Induction. *Front. Microbiol.* **8,** 1854 (2017).

57. Choi, H. J., Park, H., Kang, S., Lee E., Lee, T. A., Ra E. A. Human cytomegalovirus-encoded US9 targets MAVS and STING signaling to evade type i interferon immune responses. *Nat. Commun.* **9,** 1–16 (2018).

58. Castanier, C. & Arnoult, D. Mitochondrial localization of viral proteins as a means to subvert host defense ☆. *Biochim. Biophys. Acta* **1813,** 575–583 (2011).

59. Boya, P., Pauleau, A., Poncet, D., Gonzalez-Polo R. A., Zamzami N., Kroemer G. Viral proteins targeting mitochondria: Controlling cell death. *Biochim. Biophys. Acta.* **1659,** 178–189 (2004).

60. Magalhaes, A. C., Ferreira, A. R., Gomes, S., Vieira, M., Gouveia, A., Valença, I., Islinger, M., Nascimento R., Schrader, M., Kagan J. C. & Ribeiro, D. Peroxisomes are platforms for cytomegalovirus' evasion from the cellular immune response. *Sci. Rep.* **6,** 26028 (2016).

61. Longo, P. a, Kavran, J. M., Kim, M. & Leahy, D. J. Transient Mammalian Cell Transfection wtih Polyethylenimine. *Methods Enzymol.* **529,** 227–240 (2014).

62. Ferreira, A. R., Magalh, A. C., Kagan, J. C. & Ribeiro, D. Hepatitis C virus NS3-4A inhibits the peroxisomal MAVS-dependent antiviral signalling response. *J. Cell. Mol. Med.* **20,** 750–757 (2016).

63. Odendall, C., Dixit, E., Stavru, F., Bierne, H., Franz, K. M., Fiegen, A., Boulant, S., Gehrke, L., Cossart,P. & Kagan, J. C. Diverse intracellular pathogens activate Type III Interferon expression from peroxisomes. *Nat Immunol.* **15,** 717–726 (2014).

64. Igci, N., Sharafi, P., Demiralp, D. O., Demiralp, C. O., Yuce, A. & Dokmeci, S. Application of Fourier transform infrared spectroscopy to biomolecular profiling of cultured fibroblast cells from Gaucher disease patients: A preliminary investigation. *Adv. Clin. Exp. Med.* **26,** 1053–1061 (2017).

65. Brian., S. C. *Fundamental of Fourier Transform Infrared Spectroscopy Second Edition*. (2011). doi:10.1002/1521-3773(20010316)40:6<9823::AID-ANIE9823>3.3.CO;2-C

66. Talari, A. C. S., Martinez, M. A. G., Movasaghi, Z., Rehman, S. & Rehman, I. U. Advances in Fourier transform infrared (FTIR) spectroscopy of biological tissues. *Appl. Spectrosc. Rev.* **52,** 456–506 (2017).

67. Movasaghi, Z., Rehman, S. & Rehman, D. I. Fourier Transform Infrared (Ftir) Spectroscopy. in *Applied Spectroscopy Reviews* **43,** 134–179 (2008).

68. Fabian, H., Jackson, M., Murphy, l., Watson, P. H., Fichtner, I. & Mantsch, H. H. A Comparative Infrared Spectroscopic Study of Human Breast Tumors and Breast Tumor Cell Xenografts. *Biospectroscopy* **1,** 37–45 (1995).

69. Eckel, R., Huo, H., Guan, H., Hu, X. & Che, X. Characteristic infrared spectroscopic patterns in the protein bands of human breast cancer tissue. *Vib. Spectrosc.* **27,** 165–173 (2001).

70. Tanner, L. B., Charmaine, C., Guan, X. L., Zhengdeng, L., Rosen, S. G. & Wenk, M. R. Lipidomics identifies a requirement for peroxisomal function during influenza virus replication. *J. Lipid Res.* **55,** 1357–1365 (2014).

71. Jean Beltran, P. M., Cook, K. C., Hashimoto, Y., Galitzine, C., Murray, l. A., Vitek, O. & Cristea, I. M. Infection-Induced Peroxisome Biogenesis Is a Metabolic Strategy for Herpesvirus Replication. *Cell Host Microbe* 1–16 (2018). doi:10.1016/j.chom.2018.09.002

72. Sychev, Z. E., Hu, A., DiMaio, T. A., Gitter, A., Camp, N. D., Noble, W. S., Wolf-Yadlin, A. & Lagunoff, M. Integrated systems biology analysis of KSHV latent infection reveals viral induction and reliance on peroxisome mediated lipid metabolism. *PLoS Pathog.* 1–28 (2017). doi:10.1371/journal.ppat.1006256

73. Gazi, E., Dwyer, J., Gardner, P., Ghanbari-Siahkali, A., Wade, A. P., Miyan, J., Lockyer, N., P., Vickerman J., C., Clarke, N. W., Shanks, J. H., Scott, L. J., Hart, C. A. & Brown, M. Applications of Fourier transform infrared microspectroscopy in studies of benign prostate and prostate cancer. A pilot study. *J. Pathol.* **201,** 99–108 (2003).

74. Shivu, B., Seshadri, S., Li, J., Oberg, K. A., Uversky, V. N. & Fink, A. L. Distinct β-sheet structure in protein aggregates determined by ATR-FTIR spectroscopy. *Biochemistry* **52,** 5176–5183

(2013).